

1 The role of radiation in organizing convection in
2 weak temperature gradient simulations

Sharon L. Sessions,¹ Stipo Sentić,¹ and Michael J. Herman,¹

Corresponding author: S. L. Sessions, Department of Physics and Geophysical Research Center,
New Mexico Institute of Mining and Technology, 801 Leroy Pl., Socorro, NM 87801, USA.
(sessions@kestrel.nmt.edu)

¹Department of Physics and Geophysical
Research Center, New Mexico Tech,
Socorro, NM, USA.

Abstract.

Using a cloud system resolving model with the large scale parameterized by the weak temperature gradient approximation, we investigated the influence of interactive versus non-interactive radiation on the characteristics of convection and convective organization. The characteristics of convecting environments are insensitive to whether radiation is interactive compared to when it is not. This is not the case for non-convecting environments; interactive radiative cooling profiles show strong cooling at the top of the boundary layer which induces a boundary layer circulation that ultimately exports moist entropy (or analogously moist static energy) from dry domains. This upgradient transport is associated with a negative gross moist stability, and it is analogous to boundary layer circulations in radiative convective equilibrium simulations of convective self-aggregation. This only occurs when radiation cools interactively. Whether radiation is static or interactive also affects the existence of multiple equilibria—steady states which either support precipitating convection or which remain completely dry depending on the initial moisture profile. Interactive radiation drastically increases the range of parameters which permit multiple equilibria compared to static radiation; this is consistent with the observation that self-aggregation in radiative-convective equilibrium simulations is more readily attained with interactive radiation. However, the existence of multiple equilibria in absence of interactive radiation suggests that other mechanisms may result in organization even in absence of interactive radiation.

1. Introduction

26 Convective organization is the phenomenon in which convection forms coherent struc-
27 tures, usually flanked by dry subsiding regions in the troposphere. It is important since
28 the spatio-temporal distribution of convection and moisture has a significant impact on
29 the global energy budget. Organized convection modulates the amount of energy radi-
30 ated upward in clear sky regions compared to the longwave radiation that is trapped by
31 water vapor. As the atmosphere warms, there is evidence for an increased tendency for
32 convection to organize. This may act as a negative feedback that cools the atmosphere
33 as the climate changes [*Khairoutdinov and Emanuel, 2010*]. Understanding the mech-
34 anisms which control the large-scale organization of tropical deep convection not only
35 helps to prepare for the consequences of climate change, but provides important clues for
36 improving parameterizations of these processes in large scale models.

37 The mechanisms thought to be responsible for organizing convection are as diverse as the
38 various manifestations of organization; the latter include tropical cyclones, convectively
39 coupled waves, and the Madden-Julian Oscillation among others. Observations and nu-
40 merical experiments have identified several important factors in convective organization.
41 These include interaction with tropical waves [*Frank and Roundy, 2006; Kiladis et al.,*
42 *2009*], cloud-radiation interactions [*Tompkins and Craig, 1998; Nilsson and Emanuel,*
43 *1999; Raymond, 2001; Bretherton et al., 2005; Nolan et al., 2007; Muller and Held,*
44 *2012; Wing and Emanuel, 2013*], sea surface temperature (SST) distributions [*Lindzen*
45 *and Nigam, 1987; Tompkins, 2001a, b; Nolan et al., 2007; Back and Bretherton, 2009*],
46 convection-moisture feedbacks [*Held et al., 1993; Tompkins, 2001b; Craig and Mack, 2013*],

47 horizontal moisture advection [*Sobel et al.*, 2007; *Wang and Sobel*, 2012; *Sessions et al.*,
48 2015], mean surface wind [*Nolan et al.*, 2007], rotation [*Bretherton et al.*, 2005; *Nolan*
49 *et al.*, 2007; *Khairoutdinov and Emanuel*, 2013; *Davis*, 2015], vertical wind shear [*Held*
50 *et al.*, 1993; *Robe and Emanuel*, 2001; *Cohen and Craig*, 2006; *Anber et al.*, 2014], and
51 cold pools [*Jeevanjee and Romps*, 2013; *Feng et al.*, 2015]. In addition, models also show
52 that convective organization is sensitive to domain size [*Bretherton et al.*, 2005; *Nolan*
53 *et al.*, 2007; *Muller and Held*, 2012], domain geometry [*Wing and Cronin*, 2015] model
54 resolution [*Muller and Held*, 2012], and cloud microphysical parameterizations [*Brether-*
55 *ton et al.*, 2005], including the terminal velocity of raindrops [*Parodi and Emanuel*, 2009].
56 The thermodynamic environment is also important for convective organization as it may
57 provide conditions which are either conducive or hostile to the development of deep con-
58 vection [*Sessions et al.*, 2015]; an example of the former is cyclogenesis associated with
59 temperature dipole anomalies in African Easterly Waves [*Raymond and Sessions*, 2007;
60 *Gjorgjievska and Raymond*, 2014; *Raymond et al.*, 2015]. Convection may also organize
61 in the absence of any obvious large-scale forcing. Spontaneous organization of convection
62 in horizontally homogeneous forcing conditions is often referred to as “self-aggregation”
63 [*Su et al.*, 2000].

64 The goal of this research is to consider the effect of interactive versus non-interactive
65 radiation and the thermodynamic environment in organizing deep tropical convection.
66 Rather than varying parameters and environmental conditions on a large domain, we im-
67 plement a small domain cloud-system resolving model (CRM) which parameterizes the
68 large-scale using the weak temperature gradient (WTG) approximation. The WTG ap-
69 proximation is based on the observation that horizontal temperature gradients are small

70 in the tropical free troposphere as a result of the redistribution of buoyancy anomalies by
71 gravity waves. WTG simulations have been used successfully to investigate various prop-
72 erties of convection and convective organization. For example, it has been implemented in
73 a simple model of the Hadley circulation [*Polvani and Sobel, 2002*], the Madden-Julian Os-
74 cillation [*Wang et al., 2013; Sentic et al., 2015*], and cyclogenesis [*Raymond and Sessions,*
75 2007].

76 The WTG approximation has also been used as a computationally inexpensive method
77 for investigating self-aggregation. Self-aggregation describes the phenomena by which
78 convection spontaneously organizes into a single region exhibiting intense precipitation
79 surrounded by an extremely dry, subsiding troposphere. It occurs on larger domains
80 which are run to radiative-convective equilibrium (RCE). Multiple equilibria occur in
81 certain smaller-domain WTG simulations in which a multiplicity of steady states arise
82 that either support persistent precipitating convection, or else remain completely dry
83 under identical forcing conditions [*Sobel et al., 2007; Sessions et al., 2010; Daleu et al.,*
84 2015a]. Multiple equilibria in WTG simulations are analogous to the dry and precipitating
85 regions in larger self-aggregated RCE domains. Thus, WTG simulations may be used to
86 investigate convective organization by identifying conditions which support or suppress
87 domain-mean convection. Suppressing convection in WTG simulations is a proxy for
88 organization since it represents the dry regions surrounding regions of active convection.

89 In addition to identifying conditions which support or suppress convection—and by
90 analogy identifying relevant mechanisms of convective organization—WTG is also an ef-
91 ficient method for characterizing convection in different thermodynamic environments, as
92 was demonstrated in *Sessions et al. [2015]*. In this work, we utilize the strategy of *Ses-*

93 *sions et al.* [2015], but rather than investigating the additional role of horizontal moisture
94 advection [as in *Sessions et al.*, 2015], we consider how interactive versus non-interactive
95 radiative cooling affects convection in different thermodynamic environments. Given that
96 nearly all 3-dimensional RCE simulations of convective organization require interactive
97 radiation for spontaneous organization [e.g. *Bretherton et al.*, 2005; *Muller and Held*,
98 2012]—the notable exception being *Tompkins* [2001b]—we hope to elucidate the role of
99 interactive radiation in the organization of tropical convection. We will explicitly test this
100 with multiple equilibria experiments using interactive and non-interactive radiative cooling
101 profiles and compare convective diagnostics with previous studies of self-aggregation.

102 The effect of interactive radiation compared to non-interactive radiation has been con-
103 sidered in previous WTG studies. *Anber et al.* [2014, 2015] investigated the convective
104 response to vertical wind shear in WTG simulations. In the first paper, *Anber et al.*
105 [2014] used a fixed radiative cooling rate of -1.5 K day^{-1} , while in the second paper they
106 examined the role of interactive radiation compared to convection evolving with a static
107 radiative cooling profile equal to the time and domain mean of the interactive case [*An-*
108 *ber et al.*, 2015]. The relevant results for this study are those relating to the unshered
109 cases. They found that interactive radiation produced much stronger vertical motion in
110 the upper troposphere which imported low moist static energy air in the mid-troposphere.
111 This resulted in an increase in normalized gross moist stability which decreased precipi-
112 tation rate. As we illustrate below, our results contrast somewhat with these studies: we
113 instead find that the interaction between radiation and the large-scale circulation occurs
114 in the lower atmosphere. Precipitation rates as well as other convective diagnostics are

115 insensitive to whether radiation is interactive. In contrast, non-precipitating steady states
 116 exhibit significant differences which affect convective organization.

117 This paper is organized as follows: In section 1.1, we briefly introduce the weak temper-
 118 ature gradient approximation and its implementation in our model. The model, different
 119 options for parameterizing radiative cooling, and numerical experiments are described in
 120 section 2. We characterize convection using several diagnostic quantities that are defined
 121 in section 3; results are presented in section 4. We discuss our results in the context of
 122 convective organization in section 5, and summarize our conclusions in section 6.

1.1. Weak temperature gradient (WTG) approximation

123 The weak temperature gradient (WTG) approximation provides a means to parameter-
 124 ize the large-scale tropical environment in limited domain simulations [*Sobel and Brether-*
 125 *ton, 2000; Raymond and Zeng, 2005*]. We use an upgraded version of the model described
 126 in *Raymond and Zeng [2005]*; model upgrades are documented in *Herman and Raymond*
 127 *[2014]*. The procedure is similar to the experiments described in *Sessions et al. [2015]*; in
 128 that work, the authors investigated how different parameterizations of horizontal moisture
 129 advection affected the characteristics of convection using static radiative cooling profiles.
 130 Here, we choose to parameterize horizontal moisture advection using lateral entrainment
 131 induced by WTG circulations (described below), and consider the effect of interactive
 132 versus non-interactive radiative cooling.

133 The prognostic equation for equivalent potential temperature, θ_e is:

$$134 \quad \frac{\partial \rho \theta_e}{\partial t} + \nabla \cdot (\rho \mathbf{v} \theta_e - K \nabla \theta_e) = \rho (S_{es} + S_{er} - S_e), \quad (1)$$

135 where ρ is the density, \mathbf{v} is the velocity, and K is the eddy mixing coefficient. S_{es} and S_{er}
 136 are sources of equivalent potential temperature from surface fluxes and radiation; S_e is
 137 the sink of θ_e due to enforcing the WTG approximation.

138 The total water mixing ratio, r_t , is governed by:

$$139 \quad \frac{\partial \rho r_t}{\partial t} + \nabla \cdot (\rho \mathbf{v} r_t - K \nabla r_t) = \rho S_{cr} + \rho(S_{rs} - S_r) \quad . \quad (2)$$

140 Here, S_{cr} is minus the conversion rate of cloud water to precipitation, S_{rs} is the source of
 141 total cloud water from surface evaporation, and S_r is a sink of total water mixing ratio
 142 that results from enforcing the WTG approximation.

143 The WTG approximation is enforced by relaxing the domain mean potential temper-
 144 ature, $\bar{\theta}$, to a reference profile which represents the large-scale, θ_0 , over a time scale t_θ .

145 This results in a potential temperature sink, S_θ :

$$146 \quad S_\theta = M(z) \frac{(\bar{\theta} - \theta_0)}{t_\theta}, \quad (3)$$

147 where $M(z) = \sin(\pi z/H)$ is a masking function which modulates the relaxation. It is
 148 only applied between the boundary layer top ($z = b$) and the tropopause ($z = H$); above
 149 H , M is set to zero.

150 The potential temperature anomaly in equation (3) generates a vertical velocity in the
 151 model—the weak temperature gradient vertical velocity—that counteracts the diabatic
 152 heating:

$$153 \quad w_{wtg} = \left(\frac{\partial \bar{\theta}}{\partial z} \right)^{-1} S_\theta \quad . \quad (4)$$

154 This vertical velocity vertically advects moisture and, via mass continuity of the WTG
 155 velocity field, entrains moisture from the surrounding environment. This contributes to

156 an external sink of total water mixing ratio (S_r in equation (2)):

$$157 \quad S_r = w_{wtg} \frac{\partial \bar{r}_t}{\partial z} + (\bar{r}_t - r_x) \frac{1}{\rho_0} \frac{\partial \rho_0 w_{wtg}}{\partial z}, \quad (5)$$

158 where the first term on the right side vertically advects moisture, and the second term
 159 laterally entrains moisture from the environment (specified by a reference profile r_{t0})
 160 according to:

$$161 \quad r_x = \begin{cases} \bar{r}_t & \text{if } \partial \rho_0 w_{wtg} / \partial z < 0 \quad (\text{detraining levels}) \\ r_{t0} & \text{if } \partial \rho_0 w_{wtg} / \partial z > 0 \quad (\text{entraining levels}) \end{cases} . \quad (6)$$

162 Enforcing the WTG approximation also contributes to a θ_e sink (S_e in equation (1)) which
 163 is analogous to equations (5) and (6) with r_t replaced by θ_e .

164 We should also point out that since WTG is not a good approximation in the boundary
 165 layer, w_{wtg} is linearly interpolated from its value at the top of the boundary layer to zero
 166 at the surface.

2. Numerical Experiments

167 In this section we describe the model parameters, the reference profiles used in the
 168 implementation of WTG, and the options for radiatively cooling the model.

2.1. Model Set Up

169 The model set up in this study is identical to that used in *Sessions et al.* [2015] and is
 170 briefly described here for self-containment.

171 All simulations are performed on two-dimensional domains with a horizontal dimension
 172 200 km and resolution of 1 km; the vertical spans 20 km with 250 m resolution. Two-
 173 dimensional domains are a good strategy for this work since the point is to understand
 174 the role of radiation in the response of convection to different thermodynamic environ-
 175 ments. The sensitivity to changes in environments and model parameters is amplified in

176 2-dimensions compared to 3D [*Wang and Sobel*, 2011], so we can meet our objective using
177 a computationally efficient approach.

178 WTG simulations typically require reference profiles for potential temperature (θ_0 in
179 equation (3)) and mixing ratio (r_{i0} in equations (5) and (6)). These are obtained by
180 time and domain averages of simulations run to radiative-convective equilibrium (RCE)
181 in non-WTG mode ($t_\theta = \infty$ in equation (3)). The profiles in this work are averages over
182 the last month of a one year long simulation; as discussed in *Sessions et al.* [2015], it is
183 unnecessary to run the RCE simulation for 1 year, but we were investigating a continuous
184 gradual warming in the model's stratosphere. This was attributed to a mass leak which
185 we have confirmed did not affect the results of the WTG simulations (and which has since
186 been fixed).

187 All simulations were run over an ocean with a surface temperature of 303 K. For RCE
188 simulations, surface winds perpendicular to the model domain are relaxed to 5 m s^{-1} , and
189 radiative cooling is permitted to adjust according to water vapor content in the domain
190 (i.e., interactive radiation, described in more detail in section 2.3). The RCE profiles of
191 potential temperature and total water mixing ratio are shown in figure 1.

192 In most WTG simulations, we increase the surface wind speed to 7 m s^{-1} to increase the
193 convective response relative to the radiative cooling. For investigating multiple equilibria,
194 we also consider wind speeds ranging from 3 to 10 m s^{-1} (described below). Radiative
195 cooling is either static (time-independent) or interactive in the WTG simulations.

196 In implementing WTG, we must specify the time scale over which the domain mean
197 potential temperature is relaxed to the reference profile (t_θ in equation (3)). Physically,
198 t_θ represents the time scale over which gravity waves counteract buoyancy anomalies in-

duced by convective heating. Typical values in WTG investigations are on the order of an
hour [Sessions et al., 2010; Wang and Sobel, 2011, 2012; Daleu et al., 2012; Anber et al.,
2014; Herman and Raymond, 2014; Wang et al., 2013; Sentic et al., 2015], though some
studies have used strict enforcement [$t_\theta = 0$, Sobel and Bretherton, 2000]. As in Sessions
et al. [2015], we choose a relaxation time scale of approximately 11 min ($1/t_\theta = 1.5 \times 10^{-3}$
 s^{-1}). We chose a shorter time scale than is typically implemented so that the modeled
convection would be sufficiently sensitive to changes in the thermodynamic environment.
Furthermore, Sessions et al. [2010] showed that shorter relaxation times permitted multiple
equilibria over a larger range of wind speeds; thus the relaxation time chosen is
conducive for investigating the effect of radiation treatment on multiple equilibria. While
this is a convenient choice, it may also be physically reasonable. The relaxation time
scale is believed to be related to the time over which gravity waves redistribute buoyancy
anomalies. Gravity wave speed is set by the depth of convection [Bretherton and
Smolarkiewicz, 1989], and 50 m s^{-1} is typical for deep convection. Given the gravity
wave speed, the time scale is set according to the distance over which the gravity waves
act. The appropriate distance is still an open question with assumptions ranging from
the size of the convective cell [Romps, 2012a, b] to the distance between convective cells
[Bretherton and Smolarkiewicz, 1989; Cohen and Craig, 2006]. A gravity wave traveling
 50 m s^{-1} will travel 33 km in 11 min, which may be physically reasonable depending on
what the appropriate length scale is.

2.2. Reference Profiles

As discussed in section 1, the thermodynamic environment can catalyze convective organization. We are interested in the convective response to changes in the thermodynamic

environment, so we prescribe perturbations to the RCE reference profiles of potential temperature and mixing ratio (figure 1) to represent different environments. This is the same strategy used in *Sessions et al.* [2015]. The experiments were motivated by *Raymond and Sessions* [2007], who found that increasing the atmospheric stability by imposing a cooling of the lower troposphere and a warming aloft resulted in higher precipitation rates and more bottom-heavy convective profiles compared to unperturbed reference profiles; similarly, they found that moistening the lower troposphere resulted in higher precipitation rates with stronger convective profiles, but the shape of the convective profile remained unchanged. *Sessions et al.* [2015] expanded those basic perturbations to include perturbations of the opposite sign—less stable and drier—as well as all combinations of perturbations applied to reference moisture and potential temperature profiles. We use an identical strategy in this work for the reference profile perturbations; the difference is that we are considering different radiation treatments. In this work, horizontal moisture advection is parameterized by lateral entrainment associated with mass continuity in the WTG velocity field (see equations 5 and 6).

The perturbations that are added to the reference profiles of potential temperature and mixing ratio (figure 1) are shown in figure 2. They are arranged so that columns going left to right represent environments with increasing moisture (moisture perturbations are indicated with a dashed line), while rows going from the bottom to the top represent increasing atmospheric stability (potential temperature profiles are shown with a solid line). The center panel (figure 2e) represents the unperturbed environment. The symbols in the upper right of each panel are geometric representations of the atmospheric conditions:

1. upright triangles (geometrically more stable shapes) represent more stable θ profiles;

244 2. neutrally stable squares represent unperturbed θ profiles;

245 3. inverted triangles (geometrically unstable shapes) correspond to less stable θ profiles.

246 The shading corresponds to the moisture perturbations; in analogy with a glass of water:

247 1. empty is drier;

248 2. half-filled indicates unperturbed r_t profiles;

249 3. solid is moister.

250 We also use a bulls-eye to easily distinguish the case where neither θ or r_t is perturbed.

251 The perturbations shown in figure 2 are identical to those in *Raymond and Sessions*
 252 [2007] and *Sessions et al.* [2015]. Specifically, we add perturbations of magnitude $\Delta\theta$ at
 253 height h to the RCE θ profile, where $\Delta\theta$ is given by:

$$254 \quad \Delta\theta = \delta\theta \left(\frac{z}{h}\right)^2 e^{[2(1-z/h)]} \quad , \quad (7)$$

255 where z is the altitude. More stable environments in figure 2 have $\delta\theta = -2$ K at $h = 3$ km
 256 and $\delta\theta = 2$ K at $h = 10$ km (cooling below and warming aloft); less stable environments
 257 add perturbations of the same magnitude with opposite signs. Moisture perturbations are
 258 given by a form identical to equation 7 but with $\delta\theta$ replaced by δr_t ; $\delta r_t = \pm 1.0$ g kg⁻¹ at
 259 $h = 3$ km.

260 As in *Sessions et al.* [2015], the experimental design prescribes a time dependent ref-
 261 erence profile with the first month of the experiment given by the unperturbed RCE
 262 reference profiles, the second month perturbs *either* θ_0 or r_{t0} , and the third month per-
 263 turbs *both* θ_0 and r_{t0} . All possible combinations and sequences of perturbations generate
 264 a complete representation of the environmental profiles represented by the perturbations
 265 in figure 2. The time dependent behavior in this work is very similar to the results shown

266 in *Sessions et al.* [2015]; thus, we refer to that paper for details of time-dependent design
267 and results (those details are not essential for the results presented here).

2.3. Radiative cooling options

268 The treatment of radiation in CRMs can have a significant impact on the modeled
269 convection. For example, *Cohen and Craig* [2006] consider the effect of different radiative
270 cooling rates on convective properties in RCE simulations; the magnitude of radiative
271 cooling in these experiments was shown to affect the spatial distribution of convection.
272 Large-scale RCE simulations also show that radiative cooling—whether it is fixed or else
273 cools interactively with the thermodynamic state—has a major impact on the ability of
274 convection in a model to organize [*Tompkins and Craig*, 1998; *Bretherton et al.*, 2005;
275 *Muller and Held*, 2012; *Wing and Emanuel*, 2013; *Davis*, 2015].

276 We consider three options for radiation treatments:

- 277 1. fixed cooling rate of -1.8 K day^{-1} through the troposphere; this is the “fixed” option;
- 278 2. time-independent cooling profile generated from the RCE; since this option isn’t at
279 a fixed rate, but is static in time, we call this the “static” option;
- 280 3. interactive radiation in which the radiative cooling profile is calculated interactively
281 by the model according to the column thermodynamics including the water vapor content;
282 this is the “interactive” option.

283 The interactive radiation scheme uses an updated version of the toy model described
284 in Raymond and Torres (1998). It calculates the radiative source term for equivalent
285 potential temperature (S_{er} in equation 1) according to the net flux (upward stream minus
286 downward stream) of infrared radiation. The spectrum of radiation is approximated by
287 11 water vapor bands (only six were used in Raymond and Torres 1998), one carbon

288 dioxide band, and one band that accounts for atmospheric infrared windows and possible
289 continuum absorption by water vapor. Radiative cooling is due to longwave radiation;
290 shortwave radiation is not parameterized. Clouds increase absorptivity in proportion
291 to cloud water content, and scattering is neglected. Though the approximations are
292 significant, this computationally inexpensive scheme reproduced reasonable heating rates
293 over a wide range of atmospheric conditions when it was compared to the National Center
294 for Atmospheric Research CCM2 radiation model (see Raymond and Torres 1998 for
295 further details of the radiation model).

296 The static radiative cooling profile eliminates the radiation interactions and thus isolates
297 effects of radiation compared to other mechanisms, yet it maintains a cooling profile that is
298 native to the model environment (it is given by the time and horizontal domain average of
299 the interactive scheme over the last 30 days of the RCE simulation). On the other hand,
300 many WTG simulations use a fixed radiative cooling profile (for example, see a recent
301 intercomparison of large-scale parameterizations, including WTG, *Daleu et al.* [2015a]),
302 and the shape of the cooling profile may also affect the characteristics of convection.
303 Including both options can inform the extent to which the shape of the cooling profile
304 affects convection (via its effect on the source of equivalent potential temperature, S_{er} in
305 equation 1). We choose -1.8 K day^{-1} for the fixed option because this is the mean cooling
306 rate of the radiative cooling profile in the troposphere calculated from the RCE simulation.
307 In other words, vertically averaging the “static” radiative cooling profile in the lowest 15
308 km yields a net -1.8 K day^{-1} . Both the static and fixed cooling profiles are shown in each
309 panel of figure 3 (these are unchanged across all thermodynamic environments).

310 Figure 3 shows the radiative cooling profiles for all choices of radiation treatment in all
311 of the reference profiles represented by the perturbations in figure 2. Note that the static
312 (blue) and fixed (black) profiles are—by design—-independent of reference environment. In-
313 teractive radiation (red), on the other hand, is highly sensitive to changes in the reference
314 potential temperature profile, but relatively insensitive to changes in the reference mois-
315 ture profile. If the potential temperature is unperturbed (figure 3d-f), the interactive
316 radiative cooling profile is nearly identical to the static cooling profile. In more stable
317 environments (figure 3a-c), there is stronger cooling in the upper troposphere where the
318 warm anomalies are prescribed, and less cooling in the lower troposphere where there are
319 cool anomalies. In less stable environments (figure 3g-i), the interactive cooling profile
320 changes drastically, with strong cooling in the boundary layer, and weak cooling aloft
321 compared to the static cooling profile. The cooling profiles generated with interactive ra-
322 diation compared to static or fixed cooling profiles have profound effects on the convective
323 diagnostics; this will be discussed in more detail in sections 4 and 5. The dashed red lines
324 in figure 3b,c,e,f are interactive cooling profiles from simulations that are initiated with
325 dry tropospheres; these are results from the multiple equilibria simulations described in
326 sections 2.4 and 4.3.

327 These cooling profiles are very different from those obtained in *Anber et al.* [2015], who
328 considered the effect of wind shear and static versus interactive radiation on convection in
329 WTG simulations. In their figure 2, the radiative cooling profiles show a cooling of about
330 1 K day^{-1} from the surface to about 12 km only for weak surface fluxes; stronger surface
331 fluxes generate cooling patterns reminiscent of stratiform clouds with strong cooling (-8 to
332 -12 K day^{-1}) at about 12 km with strong warming ($5-7 \text{ K day}^{-1}$) at an approximate cloud

333 base of 8 km. Radiative cooling is negligible below 7 km in these cases. Somewhat similar
334 cooling profiles (at least in the vicinity of the tropopause) are reported for disturbed
335 regions in idealized RCE simulations [*Posselt et al., 2008; Stephens et al., 2008*]. In
336 contrast, figure 3 shows cooling throughout the troposphere with magnitudes ranging from
337 1-4 K day⁻¹ in convecting environments; the strongest cooling—about 5 K day⁻¹—occurs
338 at the top of the boundary layer in domains with suppressed convection. Although not
339 in perfect agreement, these cooling profiles reproduce gross features of what is observed
340 in nature [*McFarlane et al., 2007*]. Convecting profiles also agree with domain mean
341 cooling profiles in the idealized RCE simulations [*Stephens et al., 2008*], while the dry
342 cooling profiles resemble those from the undisturbed regions in idealized RCE simulations
343 [*Posselt et al., 2008*].

2.4. Multiple equilibria

344 The pursuit of multiple equilibria in limited domain WTG simulations represents one
345 strategy for investigating convective organization that occurs on larger scales. If the
346 organization is characterized by strong moisture gradients in which regions of intensely
347 precipitating convection is surrounded by regions of strong descent exhibiting a tropo-
348 sphere depleted of moisture, then multiple equilibria represents either the region of strong
349 convection or the region of strong descent. We hypothesize that parameters or mecha-
350 nisms which support multiple equilibria in WTG simulations are indicative of conditions
351 that promote convective organization.

352 In order to investigate multiple equilibria, we perform parallel numerical experiments:
353 in one set the tropospheric moisture is initialized with the RCE mixing ratio profile;
354 in the other set, the initial tropospheric moisture is set to zero everywhere. All other

355 boundary and prescribed forcing conditions are identical. Multiple equilibria exist if
356 the initially moist troposphere sustains precipitating convection while the initially dry
357 simulation remains dry with descent in the free troposphere. If the initially dry simulation
358 develops precipitating convection, or if the initially moist simulation dries and exhibits
359 descent in the steady state, then a single equilibrium exists. Varying model parameters
360 so that we can identify circumstances which either support or suppress multiple equilibria
361 can provide insight to mechanisms that are important for convective organization.

362 In this paper, we focus on the role of the thermodynamic environment and radiation
363 treatment on convective organization. *Sessions et al.* [2015] performed a limited num-
364 ber of multiple equilibria experiments in different thermodynamic environments. In that
365 work, the authors considered multiple equilibria in more stable and more moist environ-
366 ments (with perturbations identical to those in figure 2b,c,f), as well as in an environment
367 with unperturbed thermodynamic profiles (i.e., figures 1 and 2e). Using static radiation
368 (with the radiative cooling profile set by the RCE cooling profile), the authors considered
369 how different parameterizations of horizontal moisture advection affected the existence of
370 multiple equilibria. They found that their model—the same one used in this study—only
371 supported multiple equilibria in an unperturbed environment and only when horizontal
372 moisture advection was parameterized using lateral entrainment. In this work, we re-
373 strict our moisture treatment to lateral entrainment, and we permit radiation to cool
374 interactively.

375 For this set of experiments, we restrict our radiation treatment to the static and inter-
376 active cases (as we will show in section 4, there is minimal difference in the characteristics
377 of convection between the static and fixed profiles, so we don't perform multiple equilibria

378 experiments with fixed radiative cooling). We also only consider environments which are
379 less likely to support the dry equilibrium: more moist and/or more stable (corresponding
380 to RCE perturbations shown in figure 2b,c,f). We repeat initially dry and moist sim-
381 ulations using wind speeds ranging from 3-10 m s⁻¹ to identify a range of parameters
382 which support multiple equilibria, and to compare how that range changes with radiation
383 treatment in different thermodynamic environments.

3. Diagnosing convection

384 In addition to determining the conditions which permit multiple equilibria, it is useful
385 to diagnose the characteristics of convection in different thermodynamic environments.
386 *Sessions et al.* [2015] identified a set of diagnostics that not only served to quantify the
387 characteristics of convection, but also elucidated the relationships between the convective
388 environment and the precipitation produced by the convection. We will use the same
389 diagnostics for this work, and they are described below.

390 The primary diagnostic used to characterize convection is the space and time averaged
391 precipitation rate. To zeroth order, it indicates conditions which permit or suppress con-
392 vection, and provides a measure of the strength of convection when the precipitation rate
393 is non-zero. By itself, however, precipitation rate is a limited diagnostic since different
394 vertical and horizontal distributions of convective updrafts may produce similar precipi-
395 tation rates. Consequently, we also calculate the saturation fraction, an instability index,
396 a measure of deep convective inhibition, and the normalized gross moist stability. These
397 are all defined below. It is also useful to consider vertical profiles of potential temperature
398 and mixing ratio anomalies, as well as vertical profiles of mass flux. The mass flux is
399 calculated as the product of the density and total vertical velocity. In WTG simulations,

400 the total velocity is the sum of resolved and WTG velocity fields. In taking the domain
 401 average, the contribution from the resolved velocity is zero since what goes up must come
 402 down. Consequently, the only non-zero contribution to the mass flux is from the WTG
 403 vertical velocity:

$$404 \quad \text{mass flux} = \rho w_{wtg} \quad . \quad (8)$$

405 The saturation fraction provides a measure of the moisture contained in the model do-
 406 main. It is the vertically integrated precipitable water divided by the vertically integrated
 407 saturated precipitable water. As in *Sessions et al.* [2015], we approximate it as

$$408 \quad S = \frac{\int \rho(s - s_d) dz}{\int \rho(s^* - s_d) dz} \quad (9)$$

409 where the vertical integrals are taken over the entire depth of the model (20 km deep).
 410 $s_d = c_p \ln(\theta/T_R)$ is the dry entropy ($c_p = 1005 \text{ J kg}^{-1}\text{K}^{-1}$ is the specific heat at constant
 411 pressure, and $T_R = 300 \text{ K}$ is a constant reference temperature), s is the moist entropy
 412 (with θ replaced by θ_e in the dry entropy definition), and s^* is the saturated moist entropy.

413 Perturbations applied to the reference potential temperature profiles change the atmo-
 414 spheric stability. We quantify this by an instability index, Δs^* [*Raymond et al.*, 2011;
 415 *Gjorgjievska and Raymond*, 2014; *Sessions et al.*, 2015], defined as

$$416 \quad \Delta s^* = s_{low}^* - s_{high}^* \quad , \quad (10)$$

417 where s_{low}^* is the domain mean saturated moist entropy in the level between 1 and 3 km,
 418 and s_{high}^* is the domain mean saturated moist entropy in the level between 5 and 7 km.
 419 At a given altitude, s^* is nearly a function of temperature only, thus the difference in the
 420 mean s^* at two levels gives a measure of the atmospheric stability that often co-varies

421 with negative lower tropospheric convective available potential energy (CAPE). Smaller
 422 values of Δs^* correspond to more stable environments; larger values are more unstable.

423 Deep convective inhibition (DCIN) expresses the likelihood that low-level parcels will
 424 reach their respective levels of free convection [*Raymond et al.*, 2003]. It is defined as

$$425 \quad \text{DCIN} = s_t^* - s_b, \quad (11)$$

426 where s_t^* is the threshold entropy for convection given by the average of the saturated
 427 moist entropy in the layer between 1750 and 2000 m; s_b is the boundary layer moist
 428 entropy, averaged from the surface to 1750 m. Small or negative values of DCIN are
 429 conducive to developing deep convection; large values inhibit it.

430 Finally, we also calculate the normalized gross moist stability (NGMS). First introduced
 431 by *Neelin and Held* [1987], the gross moist stability provides a measure of the response of
 432 convection to the large-scale forcing. It is defined as the export of some quantity that is
 433 approximately conserved in moist processes (usually moist static energy or moist entropy)
 434 divided by a measure of the strength of the convection [see the review by *Raymond et al.*,
 435 2009]. We define NGMS, Γ , as the export of moist entropy divided by the lateral import
 436 of moisture:

$$437 \quad \Gamma = \frac{T_R [\nabla_h \cdot (\rho s \mathbf{v})]}{-L [\nabla_h \cdot (\rho r_t \mathbf{v})]} = \frac{T_r \int \nabla_h \cdot (\rho s \mathbf{v}) dz}{-L \int \nabla_h \cdot (\rho r_t \mathbf{v}) dz}. \quad (12)$$

438 The square brackets signify a vertical integral over the troposphere and ∇_h is the horizontal
 439 divergence operator. $T_R = 300$ K is a reference temperature, and $L = 2.833 \times 10^6$ J kg⁻¹
 440 is the sum of the latent heats of condensation and freezing; these constants are included to
 441 non-dimensionalize Γ . The temperature profile of the reference environment has a strong
 442 influence on the shape of the vertical mass flux profile [*Raymond and Sessions*, 2007;

443 *Gjorgjievska and Raymond, 2014; Sessions et al., 2015*]; this in turn controls the lateral
 444 entrainment and detrainment of moisture and moist entropy (denominator and numerator
 445 in equation 12, respectively), and thus controls the magnitude of the precipitation rate. In
 446 the steady state, the numerator in equation 12 is equal to the net entropy forcing ($F_S - R$,
 447 where F_S is the surface moist entropy flux due to surface heat and moisture fluxes, and
 448 R is the vertically integrated entropy sink per unit mass due to radiation); while the
 449 denominator is equal to the net precipitation ($P - E$, where P is the precipitation rate
 450 and E is the evaporation). Together, the steady state NGMS is inversely related to the
 451 net precipitation:

$$452 \quad \Gamma = \frac{T_R(F_S - R)}{L(P - E)} \quad , \quad (13)$$

453 [*Raymond et al., 2007*]. For most experiments, the SST is held constant and the surface
 454 wind speed is relaxed to a constant value over a timescale of a few hours so that F_S
 455 is approximately constant; if radiation is not interactive, then R is also constant and
 456 $P - E \propto 1/\Gamma$ so that the net precipitation is entirely controlled by NGMS (which is
 457 indirectly controlled by the vertical mass flux). Permitting radiation to cool interactively
 458 may adjust R , though we still expect a strong correlation between the net precipitation
 459 and the inverse NGMS.

4. Results

460 The diagnostic quantities in this work are either given as vertical profiles or scalar
 461 variables. In all cases, the computational domain is horizontally averaged, and a time
 462 average is taken over the last two weeks of the one month segment of the simulation that
 463 represents a specific thermodynamic environment. Because a single numerical simulation

464 runs for 90 days with a perturbation added in 30 day intervals, the last hour of the 30 day
465 increment is excluded in the time average to avoid including conditions representative of
466 the newly perturbed environment. *Sessions et al.* [2015] showed time series of precipitation
467 rate for all combinations of perturbations used in that study; their figures 6-8 are identical
468 to the static radiation experiments in this paper so we refer to that work for details
469 regarding the time dependence (there are no significant differences, so we consider only
470 the time mean quantities). However, we do point out a caveat from that work that
471 holds here: in most cases, two weeks is sufficient for the model to equilibrate following a
472 perturbation applied to the reference profiles. However, if horizontal moisture advection is
473 parameterized by lateral entrainment (as it is in this work), then perturbing the reference
474 θ toward a less stable environment results in a gradual decrease in free tropospheric
475 moisture. The reason for this is that lateral entrainment only permits environmental
476 moisture to enter the domain, no removal of moisture occurs at detraining levels (see the
477 second term in equation 5); thus, the only mechanism for the removal of moisture from the
478 model domain is radiative subsidence down the moisture gradient. This relatively slow
479 process means that the model may not quite be in a statistically steady state during the 2
480 week period for which the time averages are taken. However, as in *Sessions et al.* [2015],
481 the difference between the almost-steady state and the true steady state values are small
482 compared to the differences between different thermodynamic environments, so we analyze
483 the diagnostics as they are, keeping this caveat in mind. Although the time-dependent
484 results in *Sessions et al.* [2015] were shown for static radiation, interactive radiation shows
485 similar behavior (not shown) and thus the discussion holds for all the simulations which
486 become less stable (all other perturbations adjust quickly).

4.1. Vertical profiles

487 In order to determine the extent to which the model domain adopts the thermody-
488 namic conditions of the reference environment, we display the potential temperature and
489 mixing ratio anomalies for each reference environment (figures 4 and 5). The imposed
490 perturbations are shown with thin black lines; different colors correspond to different ra-
491 diative cooling treatments. Note that throughout the free troposphere (from the top of
492 the boundary layer at 1 km to the 15 km tropopause) the model-derived θ anomalies are
493 nearly identical to the imposed anomalies; this is an expected consequence of enforcing
494 the WTG approximation. The only significant difference in the model's θ anomalies from
495 the imposed occur when the environment is both more moist and more stable (figure 4c).
496 In this case the model is warmer in a layer between 1 and 9 km; this is likely a consequence
497 of the latent heating due to the strong convection in this layer (compare with the vertical
498 mass flux in figure 6).

499 We would also like to point out that more stable environments (figure 4a-c) have very
500 cool boundary layers while less stable environments (figure 4g-i) have relatively warmer
501 boundary layers. This was also demonstrated in *Sessions et al.* [2015]; in fact, the blue
502 lines corresponding to static radiation in this paper are identical to the blue lines in that
503 paper (in both papers, blue lines represent simulations with static radiation and laterally
504 entrained moisture). There is negligible difference in θ anomalies between fixed and static
505 radiation, though we see that the boundary layer is cooler when interactive radiation is
506 used in less stable environments compared to fixed or static cooling profiles (cf., figure
507 4g-i).

508 In contrast, the mixing ratio anomalies in figure 5 show a much greater range of vari-
509 ability compared to the imposed reference anomalies. Note that the horizontal axes are
510 different in figure 5: panels a-f range from -2 to 2 g kg⁻¹, panels g-i range from -10 to 4
511 g kg⁻¹ (all tick marks are in 2 g kg⁻¹ intervals). There are three important observations
512 regarding the domain mean moisture in different environments with different radiation
513 treatments:

- 514 1. moisture anomalies are more influenced by θ perturbations than r_t perturbations,
- 515 2. less stable environments severely dry the troposphere,
- 516 3. there are no obvious significant differences between radiation treatments, except
517 interactive radiation more thoroughly evacuates domain moisture in less stable environ-
518 ments (5g-i) than do static or fixed radiation. It turns out that this is more important
519 than we would guess.

520 The first two observations are consistent with the results from *Sessions et al.* [2015].
521 In more stable environments (figure 5a-c), there are positive moisture anomalies in the
522 free troposphere, even in drier environments (figure 5a). The depth and magnitude of
523 the positive moisture anomalies increase when more moisture is available from the en-
524 vironment. Less stable environments (figure 5g-i) exhibit extremely negative moisture
525 anomalies, even in moister environments. When radiative cooling is interactive, there is
526 drying through an even deeper layer; the boundary layer is not as moist (non-interactive
527 radiation, on the contrary, shows a 2 g kg⁻¹ positive moisture anomaly in the boundary
528 layer), and the 1 km layer just above the boundary layer is devoid of moisture.

529 With respect to differences in radiation treatments, we note that in most cases, moisture
530 anomalies are very similar with two exceptions:

531 1. as discussed above, there is more drying in less stable environments when radiation
532 cools interactively.

533 2. There is almost no difference in the non-interactive cooling profiles (static versus
534 fixed), except in a drier environment with an unperturbed reference θ profile (figure 5d).

535 The second exception is seen in figure 5d. In this case, the interactive radiative cooling
536 profile produces moisture anomalies very similar to those produced with the static cooling
537 profile; a fixed cooling profile, on the other hand, produces a larger dry anomaly at 3 km
538 and almost no drying in the 1 km layer just above the boundary layer. The latter effect
539 results from the shallow convection evident in the fixed radiation case (see figure 6d).

540 Vertical mass flux profiles are shown in figure 6. As in the moisture anomalies shown
541 in figure 5 and in *Sessions et al.* [2015], we note that the shape of each mass flux profile
542 is primarily governed by the atmospheric stability, with weaker influences by atmospheric
543 moisture and radiation treatment. More stable environments generate more “bottom-
544 heavy” convective profiles, while less stable environments suppress convection altogether.
545 These results are discussed in detail in *Sessions et al.* [2015]; here we focus on the effects
546 of radiation.

547 There is very little difference between interactive and static mass flux profiles in more
548 stable environments (compare red and blue lines in figure 6a-c) despite differences in
549 radiative cooling profiles (figure 3a-c) where interactive radiation exhibits stronger cooling
550 in the upper troposphere and weaker cooling in the lower troposphere compared to the
551 static cooling profile. In contrast, the biggest difference between static and fixed radiative
552 cooling profiles is seen in a more stable environment (compare blue and black lines in
553 figures 3 and 6a-c). When there is uniform radiative cooling below 12 km (fixed at -1.8 K

554 day⁻¹), the vertical mass flux is weaker compared to imposing the RCE cooling profile.
555 Independent of radiation treatment, the strength of the vertical mass flux in a more
556 stable environment with bottom heavy convection is quite sensitive to the environmental
557 moisture profile; more moist environments have much stronger updrafts, with domain
558 mean maxima ranging from 0.08 to nearly 0.1 kg m⁻²s⁻¹ (all horizontal tick marks denote
559 increments of 0.02 kg m⁻²s⁻¹), while drier environments produce maxima of only 0.01-0.02
560 kg m⁻²s⁻¹.

561 If the atmospheric stability is unperturbed (figure 6d-f), then the environmental mois-
562 ture represented by the reference r_t profile governs the strength of convection. In this case,
563 drier environments produce weak vertical motion through the troposphere (it is very weak
564 when the cooling rate is fixed), while there is upward motion in the upper troposphere
565 and descent in the lower troposphere if the reference moisture profile is unperturbed or
566 moister (figure 6e,f). This case also shows a distinction between radiation treatments:
567 the radiative cooling profiles are nearly identical for static and interactive radiation (see
568 figure 3d-f), and the mass flux profiles are similar. The fixed cooling profile obviously
569 differs (it is not as cool above 5 km, but it is cooler below; see figure 3), as does the level
570 of convergence according to the mass flux profiles. Positive mass flux indicates upward
571 motion while negative value indicate descent; by mass continuity, there will be conver-
572 gence wherever mass flux is increasing with altitude. It is interesting to note that the
573 level that separates upward motion from descent (within the layer of convergence) for the
574 static and interactive radiative cooling profile occurs at about 3 km; it is located at 5
575 km when fixed radiative cooling is prescribed. Since the convergence affects the lateral
576 entrainment of moisture and moist entropy (for example, see equation 5), this is likely

577 to affect the convection and the corresponding diagnostics. We discuss this in the next
578 subsection.

579 Finally, we compare the radiation treatments in less stable environments. In this case,
580 there is little difference between the static and fixed cooling profiles; they both exhibit
581 descent throughout the free troposphere and weak upward motion in the boundary layer.
582 In contrast, interactive radiation generates descent all the way to the surface. Although
583 the weak circulation produced when radiation is non-interactive may seem insignificant,
584 this has profound consequences with respect to mechanisms responsible for organizing
585 convection.

586 One more thing to point out in the context of the mass flux profiles are the dashed
587 lines in figure 6b,c,e,f. These correspond to mass flux profiles which were initiated with
588 zero tropospheric moisture (the multiple equilibria simulations). These will be discussed
589 in more detail in section 4.3.

4.2. Diagnostic Relationships

590 In order to better understand how convection responds to changes in the environment–
591 and how interactive radiation affects that response—it is useful to consider the relationships
592 between the diagnostic quantities which characterize the convection. The precipitation
593 rate provides a meaningful measure for the strength of convection. In figure 7, we show
594 scatter plots of precipitation rate as a function of saturation fraction, instability index,
595 NGMS, and DCIN (all defined in section 3). The symbols correspond to the reference
596 environments (figures 1 and 2), and the colors correspond to different radiation treatments.

597 As expected, the precipitation rate varies strongly with the domain mean saturation
598 fraction; this agrees qualitatively with observations [*Bretherton et al.*, 2004; *Peters and*

599 *Neelin, 2006; Raymond et al., 2009; Masunaga, 2012*] and modeling studies [*Raymond*
600 *et al., 2007, 2015; Daleu et al., 2015b*]. The results also agree with *Sessions et al. [2015]*:
601 more stable environments (indicated by upright triangles) exhibit higher saturation frac-
602 tions and stronger precipitation rates, especially in moister environments, while less stable
603 environments (denoted by inverted triangles) suppress deep convection and produce ex-
604 tremely low saturation fraction values with zero precipitation rates. This holds for all
605 radiation options. *Sessions et al. [2015]* showed that the extremely low saturation frac-
606 tions in less stable environments were observed only when horizontal moisture advection
607 was parameterized via lateral entrainment of moisture (as is done in this study); it is
608 a result of radiatively driven subsidence down the moisture gradient with no sources of
609 moisture to offset the drying. Thus, the only source of moisture in the entire column is a
610 result of surface evaporation which moistens the boundary layer. Note that when radia-
611 tive cooling is interactive (red colors in figure 7), the saturation fraction is even smaller.
612 This is because the radiatively-driven subsidence extends all the way to the surface: the
613 vertical mass flux shows descent in the boundary layer only with interactive radiation (see
614 red profiles in figure 6g-i). This is a consequence of the extreme cooling at the top of the
615 boundary layer (figure 3g-i) which results in less moistening in the boundary layer (figure
616 5g-i) compared to non-interactive radiative cooling profiles. It appears that differences in
617 radiation treatments are most significant in situations which suppress deep convection.

618 The instability index quantifies the atmospheric stability. Figure 7b shows that lower
619 values of the instability index result in higher precipitation rates; higher values com-
620 pletely inhibit precipitating convection. The lines shown connect conditions having the
621 same reference moisture perturbations (i.e. solid lines connect experiments with different

622 perturbations applied to the potential temperature, but the moisture profile remains un-
623 perturbed; dashed and dotted lines have moist anomalies, $r_{RCE} + \delta r_t$, or dry anomalies,
624 $r_{RCE} - \delta r_t$). The main observations to note are

- 625 1. the strong dependence of precipitation rate on instability index, and
- 626 2. the sensitivity of precipitation rate on the environmental moisture with a given
627 instability index.

628 The latter observation is most apparent for a low instability index (corresponding to
629 a more stable environment); moister environments (filled upright triangles) exhibit much
630 higher precipitation rates than unperturbed (half-filled triangles) or drier (empty trian-
631 gles) environments.

632 The NGMS is a diagnostic that measures the convective response to changes in the
633 large-scale forcing. In the steady state, it is inversely proportional to the net precipitation
634 (see equation 13). Figure 7c shows the relationship between the precipitation rate and the
635 steady state NGMS. The inversely proportional relationship is immediately apparent with
636 large values of precipitation rates occurring for small, positive values of NGMS. There are
637 a few caveats to this figure, however. The first is that this relationship holds for constant
638 surface fluxes and radiative cooling (i.e., numerator in equation 13). While the surface
639 fluxes are the same for all of the experiments shown (the surface wind speeds and SSTs
640 are the same), we might expect that the vertically integrated radiative cooling may result
641 in slight differences for different radiation treatments. This is not observed because,
642 despite the different radiative cooling profiles in convecting environments, the vertically
643 integrated net cooling is approximately the same. The fixed cooling rate (-1.8 K day^{-1})
644 is explicitly chosen to have a value that matches the vertically integrated value of the

645 static profile. We have less control over the vertical integral of the interactive radiative
646 cooling profile; however, it is nearly identical to the static profile if the reference potential
647 temperature profile is unperturbed (figure 3d-f), and the excess cooling aloft in more
648 stable environments seems to be offset by the reduced cooling in the lower troposphere.
649 In other words, despite the differences in the radiative cooling profiles for the radiation
650 treatments in environments which support convection, the vertically integrated radiative
651 source of entropy remains approximately constant ($R \approx \text{constant}$ in equation 13). Another
652 caveat is that NGMS is not always a particularly useful diagnostic. Recall that NGMS
653 is defined as the ratio of moist entropy export to moisture import. In RCE conditions—
654 or in thermodynamic environments which are close to RCE conditions—there is no net
655 import or export of either of these quantities and NGMS is undefined (zero divided by
656 zero). This can result in very large fluctuations in the instantaneous quantities and we
657 obtain very little diagnostic value in these situations. This is evident by examining the
658 bulls-eyes (representing unperturbed reference environments) in figure 7c; the values of
659 NGMS range from about 0.5 to 2.7; this reflects large fluctuations corresponding to rapid
660 transitions between import and export of the moisture and moist entropy as convection
661 evolves. Nevertheless, in conditions which have a definite tendency for either import or
662 export of moisture and moist entropy, NGMS can be very useful for diagnosing convection.

663 There is one more important observation to make regarding the NGMS in these sim-
664 ulations: that is the behavior of NGMS in non-precipitating environments. These occur
665 in less stable environments and are clearly identified by the inverted triangles along the
666 zero precipitation line in figure 7c. In non-precipitating cases, the NGMS can be either
667 small or negative [Sessions et al., 2010, 2015]. Negative values imply that both moisture

668 and moist entropy are simultaneously exported from the domain. In all non-precipitating
669 cases, moisture is exported from the domain, so whether NGMS is positive or negative de-
670 pends on whether moist entropy is imported or exported. Moist entropy is only exported
671 if radiation is interactive: interactive radiation induces strong radiative subsidence which
672 extends through the boundary layer all the way to the surface (see the mass flux profiles
673 in figure 6g-i). In contrast, if radiation is not interactive, weak ascent in the boundary
674 layer (black and blue lines in figure 6g-i) permits weak import of moist entropy which re-
675 sults in positive NGMS. This is an extremely important result: in self-aggregation studies,
676 the dry subsiding regions in an RCE domain which exhibited convective self aggregation
677 had negative gross moist stability which served as a positive feedback that enforced the
678 aggregation [Bretherton *et al.*, 2005]. With perhaps one exception [Tompkins, 2001b], con-
679 vective organization has thus far only been demonstrated in 3-dimensional RCE domains
680 with interactive radiation [Tompkins and Craig, 1998; Bretherton *et al.*, 2005; Muller and
681 Held, 2012; Wing and Emanuel, 2013; Wing and Cronin, 2015]. This suggests that inter-
682 active radiation more readily promotes organization by extending the free tropospheric
683 descent through the boundary layer, thus enforcing conditions which suppress the develop-
684 ment of new convection in these subsiding regions, while enforcing the export of moisture
685 and moist entropy to the aggregated regions that sustain strong deep convection.

686 Finally, we examine the diagnostic, DCIN. The results are similar to those presented
687 in Sessions *et al.* [2015]: small or negative values of DCIN are conducive to developing
688 deep convection and occur with non-zero precipitation rates in figure 7d. Larger values of
689 DCIN, mostly associated with less stable environments (inverted triangles), correspond to
690 conditions which suppress deep convection and thus have zero precipitation. As discussed

691 in *Sessions et al.* [2015], the conditions most conducive for strong precipitation—more
692 stable and more moist (filled upright triangles)—have negative DCIN values that are close
693 to zero. The novel result in this study is the extremely large values of DCIN which occur
694 in unstable environments with interactive radiation (red inverted triangles in figure 7d).
695 DCIN is defined in terms of a threshold entropy (s_t^* , equation 11) and the boundary
696 layer entropy. The threshold entropy, being an average of the saturated moist entropy,
697 depends only on the temperature which is effectively fixed by the enforcement of WTG.
698 The boundary layer moist entropy, on the other hand, is a measure of the moisture in the
699 lowest 1.75 km layer. As we’ve discussed, permitting radiation to cool interactively drives
700 the subsidence all the way to the surface and effectively evacuates the moisture from the
701 domain, with the exception of trace amounts due to evaporation at the surface. This
702 results in a very small s_b , and consequently very large DCIN. This situation is especially
703 hostile to developing new convection, and thus reinforces the organization of convection
704 on the large-scale.

705 In addition to identifying how each of the diagnostics relate to precipitation rate, it
706 is useful to consider how they relate to each other. Figure 8 shows the relationships
707 between saturation fraction and instability index, saturation fraction and NGMS, NGMS
708 and DCIN, and saturation fraction and DCIN. Again, these results very closely follow
709 those reported in *Sessions et al.* [2015]:

- 710 1. There is a strong relationship between saturation fraction and instability index,
- 711 2. There is a strong relationship between saturation fraction and NGMS for high sat-
712 uration fractions and small NGMS,
- 713 3. There is not much correlation between NGMS and DCIN, and

714 4. Little correlation exists between saturation fraction and DCIN, though DCIN is
715 somewhat higher in less stable environments (inverted triangles, figure 8d).

716 The primary differences between the results in this work and *Sessions et al.* [2015] occur
717 in a less stable environment with interactive radiation (red inverted triangles). These
718 include:

- 719 1. extreme drying resulting in very low values of saturation fraction,
- 720 2. negative NGMS as a consequence of moist entropy export (rather than import when
721 non-interactive radiation is used), and
- 722 3. extremely high values of DCIN suggesting particularly hostile environments for ini-
723 tiating new convection.

724 *Sessions et al.* [2015] compared the effects of different parameterizations of horizontal
725 moisture advection. They found very little difference in the parameterizations when the
726 domain supported precipitating convection; the biggest distinctions occurred when the
727 domain was not precipitating. For example, less stable environments exhibited much lower
728 saturation fractions and higher DCIN values when moisture was laterally entrained (with
729 static radiation) compared to other parameterizations of horizontal moisture advection.
730 Figure 8 shows that this effect is amplified when radiation is interactive.

731 Although there doesn't appear to be a strong correlation between saturation fraction
732 and NGMS, if we consider only NGMS ≥ 1 (which represent good diagnostic values), then
733 there is an inverse relationship in which smaller values of NGMS correspond to higher
734 saturation fractions (see inset of figure 8b).

735 Finally, we note that there is no obvious relationship between NGMS and DCIN (figure
736 8c). As discussed in *Sessions et al.* [2015], we do not expect a strong relationship be-

737 tween these two diagnostics based on the simple analytic theory of *Raymond and Fuchs*
738 [2007]. They posited that different types of convective disturbances were destabilized by
739 different mechanisms; for example, convectively-coupled Kelvin waves are destabilized by
740 convective inhibition, whereas moisture mode disturbances (such as the Madden-Julian
741 Oscillation) are destabilized by NGMS. The real atmosphere likely has a combination of
742 these mechanisms contributing to the wide variety of convective disturbances. The point
743 here, however, is that we do not expect a correlation between NGMS and DCIN since they
744 represent different mechanisms for destabilizing convection. Nevertheless, it is interesting
745 to note that the extremely high values of DCIN are related to conditions which exhibit
746 negative gross moist stability; this is likely no accident since the descent in the boundary
747 layer is responsible for both of these observations.

4.3. Multiple Equilibria

748 Multiple equilibria occur in conditions that permit both a persistent precipitating state,
749 and one in which the free troposphere remains dry with no precipitation. The particular
750 state that is realized depends on the initial tropospheric moisture [*Sobel et al.*, 2007;
751 *Sessions et al.*, 2010; *Emanuel et al.*, 2013; *Daleu et al.*, 2015a]: initially dry tropospheres
752 remain dry while initially moist tropospheres support the continuous development and
753 decay cycle of active convection. The initial moisture profile, however, must exceed some
754 minimum threshold in order to maintain convection [*Sessions et al.*, 2010; *Emanuel et al.*,
755 2013].

756 In this study, we investigate the existence of multiple equilibria in different thermody-
757 namic environments using either static or interactive radiation. Since multiple equilibria
758 in WTG simulations are hypothesized to be a proxy for self-aggregation in larger-domain

759 RCE simulations, understanding multiple equilibria in this context will help identify (or
760 verify) mechanisms important to convective organization.

761 For this part of the study, we consider only a subset of our thermodynamic environments:

- 762 1. unperturbed RCE profiles (figure 2e),
- 763 2. more stable environments (figure 2b),
- 764 3. moister environments (figure 2f), and
- 765 4. moister, more stable environments (figure 2c).

766 The reason for only performing a subset of these is that less stable environments do
767 not support precipitation with initially moist profiles, thus, it is extremely unlikely that
768 convection will spontaneously develop when the troposphere is initially dry. Since we are
769 interested in the robustness of multiple equilibria under conditions which support strong
770 convection, we also exclude drier environments.

771 In the previous sections, we found that the most significant differences in radiation
772 treatment was between interactive and non-interactive radiative cooling; no significant
773 qualitative differences occurred as a result of the shape of the cooling profile if radiation
774 was non-interactive. Thus, we also restrict this part of the investigation to a comparison
775 between the interactive and static radiation treatments.

776 In order to determine how robust multiple equilibria are for different environments and
777 different radiation treatments, we performed parallel experiments—with one set initialized
778 with the RCE or perturbed moisture profile, and one set initially dry—for wind speeds
779 ranging from 3-10 m s^{-1} . This includes a value smaller than that used to calculate the
780 RCE state (5 m s^{-1}), and thus is expected to sustain a single, non-precipitating steady

781 state (at least with unperturbed reference profiles); and larger values which are more likely
782 to support a single precipitating steady state in unperturbed conditions.

783 Figure 9 shows results of the multiple equilibria experiments for static and interactive
784 radiation for the subset of thermodynamic environments explored. The solid lines indicate
785 simulations which were initialized with the reference moisture profile; dashed lines connect
786 experiments which were initially dry. It is clear that both the environment and radiation
787 treatment affect the existence of multiple equilibria. This is very interesting considering
788 the results of *Sessions et al.* [2015]: they found that multiple equilibria only existed with
789 a surface wind speed of 7 m s^{-1} when horizontal moisture advection was parameterized
790 using lateral entrainment (all experiments in that work used static radiation). Those
791 results are included within the blue lines in figure 9c; in this work we have included a
792 larger range of surface wind speeds (both greater than and less than 7 m s^{-1}) in order to
793 facilitate a comparison with interactive radiation.

794 Across this range of wind speeds, experiments using static radiation exhibit interesting
795 behavior in different environments compared to those using interactive radiation. In
796 particular, when a static radiative cooling profile is prescribed, figure 9a,b show that
797 a more stable environment supports precipitating convection even if the troposphere is
798 initially dry. Only a single equilibrium exists in this case (solid and dashed blue lines),
799 even at wind speeds that are weaker than that of the RCE simulation (5 m s^{-1}). It is
800 interesting to note, however, that multiple equilibria exists for static radiation simulations
801 with unperturbed θ profiles (blue lines in figure 9c,d). In these cases, the range of multiple
802 equilibria is affected by the reference moisture environment, with a moister environment
803 exhibiting multiple equilibria only when the RCE wind speed is used (see 5 m s^{-1} case

804 in figure 9d). Multiple equilibria exist over a broader range when the environment is
805 unperturbed (figure 9c).

806 Permitting radiation to interact with convection drastically changes the conditions un-
807 der which the domain supports multiple equilibria: multiple equilibria exists over a range
808 of wind speeds even in environments which are both moister and more stable (e.g., figure
809 9b). In unperturbed environments, interactive radiation supports multiple equilibria over
810 the entire range of wind speeds shown in figure 9, although it is destroyed if wind speeds
811 are increased to 15 m s^{-1} (not shown).

812 In addition to the conditions which permit multiple equilibria, is it instructive to com-
813 pare the effect of interactive radiation in convecting environments. In particular, whether
814 radiative cooling is static or interactive has very little influence on the precipitation rate.
815 This is in contrast to the results from *Anber et al.* [2015], who found that interactive
816 radiation significantly decreased precipitation rates relative to static cooling, especially at
817 higher surface fluxes (which occur for higher wind speeds in this work). They attributed
818 this to lower NGMS caused by import of air with low moist static energy at mid-levels;
819 this in turn was a consequence of increased vertical motion at upper levels, reminiscent of
820 stratiform precipitation. Though our model and the WTG implementation differs signif-
821 icantly from the Weather and Research Forecasting model used in *Anber et al.* [2015], we
822 speculate that the most significant contribution to the different behavior is a consequence
823 of the radiative cooling profiles generated by the two models (compare their figure 2 with
824 figure 3 in this paper). Their cooling profiles exhibit strong ($\sim -10 \text{ K day}^{-1}$) cooling at 12
825 km with 5 K day^{-1} heating at 8 km. The heating is likely a result of trapping longwave
826 radiation at stratiform base [see, eg., figure 1 in *Raymond and Zeng, 2000*]. The maximum

827 WTG vertical velocity occurs at 10 km—the approximate altitude that separates warming
828 below this level from cooling above. This warming heats the upper troposphere (0.5-3.5
829 K) compared to their RCE profiles. In comparison with the results from the unsheared
830 experiments using a prescribed fixed cooling rate of 1.5 K day^{-1} [Anber *et al.*, 2014], WTG
831 vertical velocities were weaker than those using the static or interactive profiles, even with
832 stronger surface fluxes. Daleu *et al.* [2015a] reported that variations in radiative cooling
833 near the tropopause in several different models influenced the precipitation rate in RCE
834 simulations; it is likely that this affect also influences WTG simulations.

835 To briefly summarize the important observations from figure 9, we note the following:

- 836 1. More stable environments only generate precipitating convection with static radia-
837 tive cooling, even with weak surface fluxes compared to RCE conditions.
- 838 2. In contrast, interactive radiation supports multiple equilibria in a wide range of
839 environments, including those with greater stability.
- 840 3. Whether radiation is static or interactive has little effect on the precipitation rate
841 in convecting environments.

842 These observations have important consequences for understanding the interplay be-
843 tween the thermodynamic environment and radiation in convective organization. This
844 will be discussed further in section 5.

845 In the mean time, it is useful to analyze the other diagnostic variables defined in section
846 3 in order to understand the difference between static and interactive radiation in the
847 context of multiple equilibria simulations. Figure 10 shows scatter plots of precipitation
848 versus saturation fraction, instability index, NGMS, and DCIN for static (left column)
849 and interactive (right column) radiative cooling. The symbols correspond to numerical

850 simulations in the different thermodynamic environments, while the colors correspond
851 to the surface wind speed, v_y , imposed perpendicular to the 2-dimensional plane of the
852 model. In some cases, multiple experiments were performed so there are several sym-
853 bols that correspond to identical conditions. As these diagnostics are all plotted against
854 precipitation rate, it is easy to distinguish the non-precipitating experiments from the
855 precipitating ones. Although we include the simulations which were initialized with zero
856 tropospheric moisture, we do not make a distinction between simulations with different
857 moisture initialization profiles. Important differences between static and interactive radi-
858 ation are indicated with gray shading.

859 In examining the difference between the static and interactive radiation diagnostics, a
860 quick glance shows generally similar behavior in all simulations which support precipita-
861 tion; the biggest differences occur in simulations with zero precipitation. For example,
862 saturation fraction values for non-precipitating simulations with interactive radiation are
863 much lower (< 0.4 , figure 10b) compared to that for static radiation (< 0.6 , figure 10a).
864 As discussed before, this is a consequence of the strong radiative cooling at the top of
865 the boundary layer (figure 3b,c,e,f) that drives descent all the way to the surface (figure
866 6b,c,e,f). The result is a much drier boundary layer and consequently smaller saturation
867 fraction.

868 At first glance, there is little difference in the relationship between precipitation rate and
869 instability index; upon closer inspection, however, we note that only the interactive radi-
870 ation simulations have experiments with zero precipitation in more stable environments
871 (compare upright triangles—smaller instability indices—in figure 10c,d). These reflect the
872 multiple equilibria observed in figure 9a,b for interactive radiation only.

873 The panels illustrating the NGMS-precipitation relationship also yield a subtle, yet
874 important difference between the effects of interactive and static radiation. For the pre-
875 cipitating states, NGMS qualitatively observes the inversely proportional relationship with
876 precipitation rate (equation 13). Note that—in contrast to the different thermodynamic
877 environments and radiation treatments seen in figure 7c—precipitating cases do not lie on
878 a single curve. The greater surface fluxes of moist entropy (F_S in equation 13) associated
879 with greater wind speeds produce higher precipitation rates for a given value of NGMS.
880 This is similar to the results shown in *Sessions et al.* [2010]. However, NGMS exhibits the
881 most significant differences between radiation treatments for the non-precipitating simu-
882 lations: static radiation produces NGMS values which are all positive, and which range
883 from slightly greater than zero to about 1.75. In contrast, NGMS takes much smaller
884 values and even becomes negative when radiation is interactive. Given the distribution
885 of gross moist stability in RCE self-aggregation studies—which show positive values in the
886 convecting regions and negative values in the dry regions [*Bretherton et al.*, 2005]—this
887 may be a significant result. We discuss this in more depth in the next section.

888 The most drastic difference between static and interactive radiation is observed in the
889 values of DCIN when the domain is devoid of convection. When static radiation is used,
890 DCIN is negative in the simulations which exhibit zero precipitation (figure 10g), sug-
891 gesting that despite the dry steady state, convection would be easy to trigger in these
892 experiments. In stark contrast are the values of DCIN when the domain is not precipitat-
893 ing but radiation is cooling interactively. In this case, DCIN lies between the considerably
894 greater values of 20 and 60 J kg⁻¹K⁻¹, suggesting a situation which would require a very
895 significant perturbation to trigger convection in these conditions. Note that the highest

996 values correspond to the lowest surface wind speeds; increasing the surface wind speed
997 increases the surface fluxes of moisture and moist entropy which increases the boundary
998 layer moist entropy (s_b in equation 11) and gradually decreases DCIN. As mentioned pre-
999 viously (but not shown), multiple equilibria do not exist with interactive radiation and a
900 surface wind speed of 15 m s^{-1} (DCIN in this case is about $2 \text{ J kg}^{-1}\text{K}^{-1}$ for an unperturbed
901 environment); it may be that a critical DCIN marks the conditions which separate the
902 precipitating states from those which severely inhibit convection. If we consider multiple
903 equilibria—or more generally dry WTG domains—as a proxy for the descending regions
904 associated with large-scale convective organization, then radiation appears to strongly
905 support existing organization by prohibiting the development of convection in the dry
906 regions via strong inhibition. We will discuss this in more detail in the next section.

907 To highlight the most important results regarding multiple equilibria in different ther-
908 modynamic environments with either static or interactive radiative cooling, we note:

909 1. Interactive radiation permits multiple equilibria even in more stable and moister
910 environments which do not support a dry equilibrium state when radiation is static.

911 2. When radiation interactively cools a dry troposphere, convection is strongly sup-
912 pressed as a consequence of radiatively driven subsidence that extends through the bound-
913 ary layer to the surface; this results in

914 (i) lower saturation fractions,

915 (ii) negative NGMS, and

916 (iii) extremely high DCIN

917 compared to simulations where a static radiative cooling profile is employed.

918 In the next section, we discuss how these observations fit within our current under-
919 standing of convective organization.

5. Discussion

920 We now discuss our results in the context of what we understand so far about the
921 mechanisms responsible for organization in models. As in previous work that analyzes
922 multiple equilibria using the WTG approximation [*Sobel et al.*, 2007; *Sessions et al.*,
923 2010; *Emanuel et al.*, 2013; *Sessions et al.*, 2015], we assume the dry and moist equilibria
924 in WTG simulations are analogous to dry, subsiding regimes and moist, precipitating
925 convective regimes, respectively, in larger domain RCE simulations. We begin with a
926 brief summary of some of the studies which analyze convective organization in cloud
927 system resolving models (CRMs).

928 *Held et al.* [1993] is perhaps one of the earliest to report convective organization in RCE
929 simulations. Using a 2-dimensional domain with interactive radiation, they found that
930 convection organized into bands of propagating convection which oscillated from westward
931 to eastward. In an attempt to remove this oscillation, they relaxed the mean zonal winds
932 to zero; in this case, the initially randomly distributed convection evolved to a stationary
933 region of convection. Imposing modest windshear destroyed all forms of organization in
934 this model. They attributed the convective organization to a memory in the moisture field
935 rather than to the low-level convergence pattern. These experiments were performed with
936 surface temperatures of 25° and 30°C; the former experiments took longer to organize,
937 exhibited slightly different character, and exhibited a smaller albedo than the experiments
938 over a warmer surface. The character of convective organization as a function of surface

939 temperature has been echoed in more recent studies [*Khairoutdinov and Emanuel*, 2010;
940 *Posselt et al.*, 2012; *Wing and Emanuel*, 2013; *Wing and Cronin*, 2015].

941 *Tompkins and Craig* [1998] performed some of the earliest 3-dimensional RCE simula-
942 tions which exhibited convective organization. Organization took the form of moist and
943 dry bands of convection in a $(100 \text{ km})^2$ domain. Both interactive surface fluxes and in-
944 teractive radiation were necessary for organization to develop; horizontally homogenizing
945 either of these fields destroyed the convective organization. This was also shown to be
946 the case in *Bretherton et al.* [2005], which is perhaps the earliest reported example of
947 convection corralled into a single, circular stationary region by virtue of the appearance
948 of an incipient dry spot with a subsiding troposphere that expands until all convection is
949 confined to a single region.

950 Most examples of convective organization using a 3-dimensional CRM have reported
951 that interactive radiation is an essential mechanism for convection to organize [*Tomp-*
952 *kins and Craig*, 1998; *Bretherton et al.*, 2005; *Stephens et al.*, 2008; *Muller and Held*,
953 2012; *Wing and Emanuel*, 2013]. A notable exception is *Tompkins* [2001b], who demon-
954 strated convective organization on a domain with rectangular “channel” geometry with
955 a horizontally homogeneous, fixed radiative cooling rate. In that work, the convection
956 organized into bands of precipitation separated by dry subsiding regions which migrated
957 either East or West. Though the organization is not as extreme as in simulations of
958 self-aggregation demonstrated in *Bretherton et al.* [2005]; *Muller and Held* [2012]; *Wing*
959 *and Emanuel* [2013], (perhaps quantifiable by the aggregation index introduced by *Tobin*
960 *et al.* [2012]), it is certainly organized with distinct dry and moist regions. In a recent
961 study of convective aggregation using channel geometry, *Wing and Cronin* [2015] used

962 the same model that was originally used to study self-aggregation that manifested as a
963 single, stationary circular patch [Bretherton *et al.*, 2005; Muller and Held, 2012; Wing
964 and Emanuel, 2013]. They found that changing the geometry of the domain reorganized
965 the convection from a single, stationary circular region to a banded structure, similar to
966 that found in Tompkins [2001b]. To evaluate mechanisms responsible for organization,
967 Wing and Cronin [2015] decomposed the frozen moist static energy budget to examine
968 the dominant feedbacks with channel geometries over SSTs ranging from 280-310 K. At
969 an SST of 300 K—the same as that used in Tompkins [2001b]—they found that while both
970 shortwave and longwave radiation were positive feedbacks in the early stages of organiza-
971 tion, surface fluxes exhibited a stronger positive feedback. Tompkins [2001b] attributed
972 organization to positive feedbacks between convection and water vapor. In another study
973 of RCE using channel geometry, Stephens *et al.* [2008] investigated radiative convective
974 feedbacks in 2- and 3-dimensional simulations with interactive and static radiative cooling.
975 Simulations with interactive radiation showed obvious signatures of organization, which
976 they attributed to radiative heating gradients induced by the existence of high clouds
977 produced in moist convecting regions, and the absence of high clouds in dry regions. It
978 is interesting to note that although organization is strong when interactive radiation is
979 invoked, there is evidence for weak organization when radiation is homogenized [see figure
980 3c in Stephens *et al.*, 2008], similar to Tompkins [2001b]. However, the organization does
981 not persist with longer model integration.

982 *Bretherton et al.* [2005] reported radiative cooling as a positive feedback which trans-
983 ported moist static energy (MSE) from the driest columns to the moistest columns. Be-
984 cause temperature gradients are weak, most of the energy transport is associated with

985 moisture transport from dry regions to moist regions, thus reinforcing the aggregated
986 state. This transport is a result of strong radiative cooling near the top of the boundary
987 layer which drives subsidence and, by mass continuity, results in export from the lowest 1
988 km of the dry regions. The export of MSE from the dry regions corresponds to negative
989 gross moist stability there. In more recent work, *Muller and Held* [2012] and *Wing and*
990 *Emanuel* [2013] specifically investigated the roles of longwave and shortwave radiation as
991 well as surface fluxes. Both of these studies report that longwave radiation is the domi-
992 nant positive feedback for the aggregated state. *Muller and Held* [2012] verified the role of
993 longwave cooling in the upgradient transport of MSE by suppressing the longwave cooling
994 from liquid condensates below 1 km; this effectively suppressed self-aggregation. A similar
995 removal of longwave cooling above 2 km or a homogenization of shortwave radiation still
996 permitted aggregation. This is in direct agreement with *Bretherton et al.* [2005]. Simi-
997 larly, *Wing and Emanuel* [2013] performed a decomposition of contributions to the frozen
998 moist static energy (FMSE) budget; they found that while shortwave radiation played an
999 important role in the initial destabilization of the RCE state to aggregation, longwave
1000 radiation was the dominant positive feedback in maintaining the aggregated state. This
1001 decompositon also highlighted the role of convergence of FMSE into the moist regions,
1002 in agreement with *Bretherton et al.* [2005] and *Muller and Held* [2012]. Similarly, in an
1003 investigation of the role of cold pools in aggregation, *Jeevanjee and Romps* [2013] reported
1004 that dry patches exhibited a dry, deep circulation and a shallow, moist circulation, both
1005 of which reinforced convective organization, in agreement with the above studies.

1006 The results presented in this paper are not only consistent with the analogous simu-
1007 lations of self-aggregation, but they help to elucidate the role of interactive radiation in

1008 convective organization. Furthermore, they provide evidence that while interactive radi-
1009 ation strongly enhances organization, it is not a requirement for its existence, which is
1010 consistent with the fact that *Tompkins* [2001b] demonstrated organized convection with
1011 homogeneous, fixed radiative cooling. To see this, consider the major results of this pa-
1012 per in the context of spontaneously organized convection in large, 3-dimensional RCE
1013 simulations:

1014 **1. The dry state exhibits strong cooling at the top of boundary layer only**
1015 **with interactive radiation** (see figure 3g-i and dry equilibria states in 3b,c,e,f). This
1016 was also reported in the dry regions of larger self-aggregated simulations [*Bretherton et al.*,
1017 2005; *Muller and Held*, 2012].

1018 **2. The boundary layer in the dry state is slightly cooler** (figure 4g-i) **and drier**
1019 **(figure 5g-i) when interactive radiation is invoked compared to prescribing a**
1020 **static profile.** The cooling is likely a consequence of the strong radiative cooling in this
1021 layer (figure 3). The drying is a consequence of subsidence; *Jeevanjee and Romps* [2013]
1022 reported a drier boundary layer in dry regions in their investigation of the role of cold
1023 pools in organizing convection.

1024 **3. The strong cooling at the top of the boundary layer in the dry state**
1025 **when interactive radiation is used results in strong descent near the top of the**
1026 **boundary layer which entrains environmental air in this layer; this descends**
1027 **to the surface where it drives net export of moist entropy (or analogously,**
1028 **MSE).** This is identical to the circulation described in *Bretherton et al.* [2005]; *Muller*
1029 *and Held* [2012]; *Jeevanjee and Romps* [2013], which results in upgradient transport of
1030 MSE, and consequently negative gross moist stability in the dry region. In contrast,

1031 prescribing a static radiative cooling profile does not permit the strong cooling at the
1032 top of the boundary layer, which changes the boundary layer circulation entirely. In the
1033 latter case, environmental air is imported at the surface and exported at the top of the
1034 boundary layer (figure 6g-i, black and blue lines). Moist entropy (or equivalently MSE)
1035 is transported down gradient and NGMS is positive.

1036 **4. The boundary layer circulation—where descent in the boundary layer re-**
1037 **sults in net export of moist entropy—maintains a dry equilibrium state even in**
1038 **conditions which support strong convection** (see, e.g., figure 9b). Interactive radi-
1039 ation effectively expands the range of parameter space which permits multiple equilibria
1040 and, by analogy, presumably also convective organization. Most RCE simulations report
1041 that interactive radiation is required for convective organization; *Tompkins* [2001b] is a
1042 notable exception.

1043 **5. Multiple equilibria exists even in the absence of interactive radiation; this**
1044 **would suggest that convection can organize with fixed, homogeneous radiative**
1045 **forcing** (see figure 9c). Although our WTG simulations with static radiation exhibit
1046 multiple equilibria in a very restricted parameter space compared to interactive radiation,
1047 multiple equilibria exist without interactive radiation (although it does not with alternate
1048 parameterizations of the large-scale, including the damped gravity wave approximation,
1049 *Daleu et al.* [2015a], and a spectral version of WTG, *Herman and Raymond* [2014]). This
1050 suggests that while interactive radiation makes it much easier to drive convection to an
1051 organized state, it is not essential. *Bretherton et al.* [2005] presented a simple model
1052 which predicted that an RCE simulation would aggregate if the sum of fitting parameters
1053 corresponding to surface-flux feedbacks and radiative feedbacks were greater than some

1054 critical value. In this simple model, it would be possible for aggregation to occur with
1055 homogeneous static radiative cooling if the surface-flux feedbacks were sufficiently strong.
1056 As mentioned above, *Tompkins* [2001b] demonstrated convective organization with fixed,
1057 homogeneous radiative cooling; while the organization is not as strong as exhibited in
1058 models with interactive radiation, it organizes nevertheless. *Stephens et al.* [2008] also
1059 provides evidence of weak (albeit temporary) organization in idealized RCE simulations
1060 with fixed radiation.

1061 If it is possible to organize convection without radiative-convective feedbacks, what
1062 other mechanisms could be responsible for the organization? In the one example we have
1063 which exhibits organization in the absence of interactive radiation, *Tompkins* [2001b]
1064 attributes organization to strong feedbacks between convection and water vapor. This
1065 explanation is consistent with the “moisture memory” proposed by *Held et al.* [1993].

1066 Recently, *Craig and Mack* [2013] presented a coarsening model for self-organization of
1067 tropical convection. The main requirement for organization is that convection in RCE can
1068 be modeled as a bistable system where drying overcomes moistening for small saturation
1069 fractions, but moistening dominates at larger saturation fractions. This requirement is
1070 supported by an earlier equilibrium study of RCE in a two-column model [*Nilsson and*
1071 *Emanuel*, 1999] as well as in studies of multiple equilibrium and self-aggregation. *Craig*
1072 *and Mack* [2013] argue that radiative cooling determines the spatial mean—but not the
1073 spatial distribution—of precipitation. Instead, the location of convection is governed by
1074 lower tropospheric moisture content (though interactive radiation may enhance moisture
1075 inhomogeneities and thus be favorable to organization). They and others [e.g. *Emanuel*
1076 *et al.*, 2013] argued that organization is most likely a result of a combination of radiative-

1077 convective interactions, water vapor-convection interactions, and surface fluxes. Accord-
1078 ing to our results as well as others, it is possible to eliminate at least one of these for
1079 convection to exhibit at least weak organization. For example, *Muller and Held* [2012]
1080 were able to obtain self-aggregation with homogeneous surface flux forcing; thus, despite
1081 the fact that homogenizing surface fluxes of moisture inhibits sharp moisture gradients
1082 that characterize the organization, radiation and water vapor interactions with convection
1083 were sufficient to permit organization.

1084 The requirement for interactive radiation likely depends on model and model parame-
1085 ters. For example, *Wing and Cronin* [2015] found that the contributions of clouds to the
1086 radiative feedbacks were sensitive to the radiation scheme invoked. *Wing and Emanuel*
1087 [2013] showed that shortwave radiation was responsible for destabilizing the domain to an
1088 organized state, while longwave radiation was the dominant mechanism responsible for
1089 maintaining the organized state. In comparison, our multiple equilibria simulations start
1090 with the analogous organized state (one dry domain and one moist); running the simu-
1091 lation determines whether those represent statistically steady states. We do not consider
1092 how the destabilization occurs in the first place, and it may be possible that interactive
1093 radiation is necessary for that, though the results from *Tompkins* [2001b] [and to a lesser
1094 degree, *Stephens et al.*, 2008] suggest otherwise. It is interesting to note that the examples
1095 which organize convection in the absence of interactive radiation use rectangular domains;
1096 perhaps the broken symmetry of the geometry—which changes the character of convection
1097 in RCE simulations even with interactive radiation [*Wing and Cronin*, 2015]—plays a role
1098 in the organization. Several studies have speculated that this is a consequence of the dom-
1099 inance of the second-mode gravity waves in initiating convection in two dimensions [e.g.,

1100 *Mapes, 2000; Bretherton et al., 2005; Stephens et al., 2008; Fuchs et al., 2014*, among oth-
1101 ers]. Furthermore, *Bretherton et al. [2005]* suggested that isotropic propagation of these
1102 gravity waves in square 3-dimensional geometries reduced the effectiveness of this insta-
1103 bility mechanism. Thus other mechanisms, perhaps related to large-scale circulations,
1104 become important.

1105 Convection can also organization as a consequence of imposed vertical wind shear,
1106 even with non-interactive radiation [*Robe and Emanuel, 2001; Cohen and Craig, 2006*].
1107 Windshear can also inhibit convective organization, as *Held et al. [1993]* demonstrated in
1108 their 2-dimensional RCE model. Perhaps reducing the symmetry of the system—either by
1109 changing the geometry of the computational domain or dynamically by imposing vertical
1110 wind shear—invokes an alternate mechanism which permits organization in the absence
1111 of interactive radiation.

1112 Dynamical asymmetries may also arise from changes in the rotational environment.
1113 Recently, *Raymond et al. [2015]* proposed a theory of tropical convection based on balanced
1114 dynamics. Observations and theories suggest that positive mid-tropospheric vorticity
1115 anomalies generate virtual temperature anomalies with cooling below and warming aloft
1116 (similar to the more stable perturbations shown in figure 2a,b,c). As shown previously
1117 [*Raymond and Sessions, 2007; Gjorgjievska and Raymond, 2014; Sessions et al., 2015*]
1118 and in this work, the more stable environment promotes more “bottom-heavy” convection
1119 which laterally entrains more moist low-level air and thus increases the precipitation rate.
1120 Similarly, a negative vorticity anomaly would generate the opposite temperature dipole
1121 anomaly which we have demonstrated can strongly suppress convection. Thus, subtle
1122 changes in the thermodynamic environment which may be induced by dynamic variations

1123 in vorticity significantly contribute to convective organization. Our results both here and
1124 in *Sessions et al.* [2015] suggest that is an important organization mechanism even in
1125 the absence of interactive radiation; however, interactive radiation strongly reinforces the
1126 organization.

1127 On a somewhat related note, *Davis* [2015] investigated the process of spontaneous orga-
1128 nization in a rotating RCE domain. His objective was to understand the origin of rotating
1129 coherent structures preceding tropical cyclogenesis. As in previous studies which invoked
1130 rotation on an RCE domain [*Bretherton et al.*, 2005; *Nolan et al.*, 2007], convection ag-
1131 gregated in the presence of interactive radiation. *Davis* [2015] also performed simulations
1132 with radiation calculated from Newtonian relaxation which was effectively a homoge-
1133 nization of the radiative cooling. Although convective aggregation was prevented in this
1134 case, the model generated moist and dry patches. Presumably, these patches could not
1135 grow in this environment without a mechanism to transport moisture upgradient. *Davis*
1136 [2015] showed that interactive radiation generated a balanced secondary circulation as a
1137 consequence of the gradient in radiative cooling between moist and dry regions (this circu-
1138 lation was absent when radiative cooling was homogenized). Profiles of relative vorticity
1139 within moist patches exhibited positive anomalies at 6 km whether or not radiation was
1140 interactive; however, the anomalies were much stronger with interactive radiation. It is
1141 interesting to note that in contrast to RCE simulations of self-aggregation in symmetric
1142 geometries without rotation [i.e. *Bretherton et al.*, 2005; *Muller and Held*, 2012; *Wing and*
1143 *Emanuel*, 2013], organization in this experiment does not initiate with the growth of an
1144 incipient dry spot. Instead, dry regions appear simultaneously with moist regions, and
1145 moist regions (associated with positive potential vorticity anomalies) merge during the

1146 organization process. Evidently, rotation changes the process of convective organization
1147 compared to simulations without rotation; perhaps rotation can be considered a type of
1148 dynamical asymmetry.

1149 Given our results in the context of previous studies, we hypothesize that

1150 1. Interactive radiation is not necessary for maintaining organization in models (al-
1151 though this may only be true in systems with reduced geometric or dynamic symmetry).

1152 2. However, interactive radiation drastically increases the parameter space which per-
1153 mits a model to exhibit organization.

1154 It is interesting that the boundary layer circulations in the dry state in this work–
1155 and the implications for upscale transport of moist entropy and thus negative gross moist
1156 stability–are in agreement with the observations made for the large-scale RCE simulations
1157 which exhibit convective organization. However, it is also interesting to consider some of
1158 the other convective diagnostics in this work. The extremely low saturation fraction and
1159 zero precipitation rate are in easy agreement with the dry regions of organized convection.
1160 A less obvious connection, however, can be made when we consider the behavior of DCIN
1161 in our model. *Tompkins* [2001b] calculated the more conventional quantity, convective
1162 inhibition (CIN), in several regions in the organized state. In the dry region, he reported
1163 high values of CIN compared to convecting regions or even dry regions which are em-
1164 bedded in a convective envelope. In this work, we found that interactive radiation has
1165 a profound effect on DCIN when radiation cools interactively compared to when it does
1166 not (see figure 7g-h). As discussed previously, interactive radiation permits the extreme
1167 drying just above and in the boundary layer which results in a nearly negligible boundary
1168 layer moist entropy and a correspondingly large DCIN. In developing stochastic and meso-

1169 scopic models for tropical convection, *Majda and Khouider* [2001] proposed CIN as an
1170 order parameter for identifying the existence of multiple radiative-convective equilibria.
1171 Considering that self-aggregation in a large-domain RCE simulation initiates organiza-
1172 tion as the growth of a single dry spot [*Bretherton et al.*, 2005; *Muller and Held*, 2012;
1173 *Wing and Emanuel*, 2013], perhaps DCIN (or CIN) represents an important parameter
1174 for diagnosing the dry regimes in convective organization. Indeed, it may be fruitful to
1175 consider a separate theory for the relationships between convective (or non-convective) di-
1176 agnostics for dry regimes separately from moist regions which sustain convection. Clearly
1177 a relationship between precipitation and other diagnostics has limited use if precipitation
1178 is zero. However, we present evidence that other diagnostic quantities, NGMS and DCIN
1179 specifically, exhibit different characteristics in the convecting regimes compared to the
1180 non-convecting regimes. It may prove to be quite informative to analyze these relation-
1181 ships in models and observational datasets in non-precipitating conditions to determine if
1182 there are any systematic tendencies which determine conditions favorable for organization.
1183 This, in turn, could be used to incorporate organization in convective parameterizations,
1184 as suggested by *Mapes and Neale* [2011] and *Tobin et al.* [2012].

6. Summary

1185 Using a cloud system resolving model with the large scale parameterized by the weak
1186 temperature gradient (WTG) approximation, we have investigated the role of radiation
1187 in organizing deep tropical convection. Convective organization in larger domain simu-
1188 lations of radiative-convective equilibrium (RCE) is characterized by regions of strong,
1189 precipitating convection with adjacent dry regions of descent.

1190 We characterize convective organization in our limited domain simulations by the ability
1191 of the model to suppress convection in the domain. This can either occur as a consequence
1192 of the thermodynamic environment, or in situations which support multiple equilibria—
1193 either a precipitating or a dry steady state—depending on the initial moisture profile. The
1194 underlying goal of this work is to examine how interactive radiation influences convec-
1195 tive organization by examining several diagnostics—including vertical profiles of radiative
1196 cooling and mass flux, and steady state values of precipitation, saturation fraction, in-
1197 stability index, normalized gross moist stability, and deep convective inhibition—both in
1198 simulations which exhibit active convection and those which suppress it.

1199 Radiative cooling in this investigation is either interacting or non-interacting. Interac-
1200 tive radiative cooling calculates the cooling rate based on the water vapor content in the
1201 model domain. The non-interactive radiative cooling profile is either calculated as the
1202 time and domain mean cooling profile from an RCE simulation, or is prescribed to be a
1203 fixed -1.8 K day^{-1} through most of the free troposphere (the rate is chosen as the vertical
1204 average of the static cooling profile).

1205 Thermodynamic environments supporting precipitating convection—represented by ei-
1206 ther unperturbed RCE or more stable reference profiles—show very little difference in the
1207 characteristics of convection when radiative cooling is interactive compared to when it
1208 is not. In contrast, the biggest differences in radiation treatments occur in dry, non-
1209 precipitating environments (which are either less stable, or which are represented by the
1210 dry equilibrium in conditions which support multiple equilibria). In a subsiding atmo-
1211 sphere, radiative cooling is strong above the boundary layer; this induces a boundary-layer
1212 circulation which imports moist entropy at the top of the boundary layer, but exports

1213 higher values of moist entropy near the surface, resulting in a net export of moist entropy
1214 (or analogously, moist static energy). This up-gradient transport of moist entropy re-
1215 sults in a negative gross moist stability, and it is analogous to the circulations induced in
1216 larger simulations of radiative convective equilibrium (RCE) in which convection exhibits
1217 spontaneous organization [referred to as self-aggregation, e.g., *Bretherton et al.*, 2005;
1218 *Muller and Held*, 2012; *Wing and Emanuel*, 2013]. As a consequence of this circulation,
1219 saturation fractions are excessively diminished and deep convective inhibition is strongly
1220 enhanced in the presence of interactive radiation, independent of thermodynamic envi-
1221 ronment, as long as convection is suppressed. It is interesting that negative gross moist
1222 stability only occurs in the steady state when radiation cools interactively.

1223 In this work, we also explored the effect of interactive radiation on the model's abil-
1224 ity to exhibit multiple equilibria. We found that interactive radiation not only permitted
1225 multiple equilibria over a larger range of surface wind speeds, but it also permitted the ex-
1226 istence of multiple equilibria in conditions which otherwise favor strong convection (more
1227 stable and more moist). In contrast, static radiative cooling in more stable environments
1228 always produced precipitation, even when surface wind speeds were reduced compared to
1229 RCE values (where we would expect radiative cooling to dominate convection).

1230 While interactive radiation strongly enhances conditions which support convective or-
1231 ganization, the existence of dry steady states—either in multiple equilibria or as a con-
1232 sequence of thermodynamic environments which are unfavorable to convection—suggests
1233 that interactive radiation is not absolutely essential for convective organization. Indeed,
1234 as others have suggested, several mechanisms are at play—radiative-convective feedbacks,
1235 precipitation-moisture feedbacks, horizontal moisture advection, and vertical wind shear—

1236 and organization is most easily achieved when some combination of these act in concert.
1237 However our results here, along with some previous work, suggest that not all have to
1238 be in effect, including what seems to be the dominant facilitator in convective organiza-
1239 tion: interactions between radiation and convection (or clear sky). However, in absence
1240 of radiative interactions, other mechanisms may require either a geometric or dynamic
1241 asymmetry to destabilize the convective domain to organization.

1242 **Acknowledgments.** We'd like to thank Chimene Daleu, David Raymond, Saska
1243 Gjorgjievska, Greg Bothun, and George Craig for helpful discussions. This work
1244 was supported by U.S. National Science Foundation Grants AGS-1056254, ATM-
1245 1021049, and AGS-1342001. The model used to generate the data is available at
1246 <http://kestrel.nmt.edu/~raymond/tools.html>. Scripts and model parameters used in this
1247 paper are available upon request from the corresponding author; please send requests via
1248 email to sessions@kestrel.nmt.edu.

References

- 1249 Anber, U., S. Wang, and A. Sobel (2014), Response of atmospheric convection to vertical
1250 wind shear: Cloud-system-resolving simulations with parameterized large-scale circula-
1251 tion. part i: Specified radiative cooling, *J. Atmos. Sci.*, *71*, 2976–2993, doi:10.1175/JAS-
1252 D-13-0320.1.
- 1253 Anber, U., S. Wang, and A. Sobel (2015), Effect of surface fluxes versus radiative cooling
1254 on tropical deep convection, *J. Atmos. Sci.*, submitted.
- 1255 Back, L. E., and C. S. Bretherton (2009), On the relationship between SST gradients,
1256 boundary layer winds, and convergence over the tropical oceans, *J. Climate*, *22*, 4182–

1257 4196, doi:10.1175/2009JCLI2392.1.

1258 Bretherton, C. S., and P. K. Smolarkiewicz (1989), Gravity waves, compensating subsi-
1259 dence and detrainment around cumulus clouds, *J. Atmos. Sci.*, *46*, 740–759.

1260 Bretherton, C. S., T. Uttal, C. W. Fairall, S. E. Yuter, R. A. Weller, D. Baumgardner,
1261 K. Comstock, R. Wood, and G. B. Raga (2004), The EPIC 2001 stratocumulus study,
1262 *Bull. Am. Meteor. Soc.*, *85*, 967–977.

1263 Bretherton, C. S., P. N. Blossey, and M. Khairoutdivnov (2005), An energy-balance anal-
1264 ysis of deep convective self-aggregation above uniform SST, *J. Atmos. Sci.*, *62*, 4273–
1265 4292.

1266 Cohen, B. G., and G. C. Craig (2006), Fluctuations in an equilibrium convective ensemble.
1267 Part II: Numerical experiments, *J. Atmos. Sci.*, *63*, 2005–2015.

1268 Craig, G. C., and J. M. Mack (2013), A coarsening model for self-organization of tropical
1269 convection, *J. Geophys. Res.*, *118*, 1–9, doi:10.1002/jgrd.50674.

1270 Daleu, C. L., S. J. Woolnough, and R. S. Plant (2012), Cloud-resolving model simulations
1271 with one- and two-way couplings via the weak temperature gradient approximation, *J.*
1272 *Atmos. Sci.*, *69*, 3683–3699, doi:10.1175/JAS-D-12-058.1.

1273 Daleu, C. L., R. S. Plant, S. J. Woolnough, S. Sessions, M. J. Herman, A. Sobel, S. Wang,
1274 D. Kim, A. Cheng, G. Bellon, P. Peyrille, F. Ferry, P. Siebesma, and L. van Uft
1275 (2015a), Intercomparison of methods of coupling between convection and large-scale
1276 circulation: I. Comparison over uniform surface conditions, *J. Adv. Model. Earth Syst.*,
1277 doi:10.1002/2015MS000468.

1278 Daleu, C. L., R. S. Plant, S. J. Woolnough, S. Sessions, M. J. Herman, A. Sobel, S. Wang,
1279 D. Kim, A. Cheng, G. Bellon, P. Peyrille, F. Ferry, P. Siebesma, and L. van Uft (2015b),

- 1280 Intercomparison of methods of coupling between convection and large-scale circulation:
1281 II. Comparison over non-uniform surface conditions, *J. of Adv. Model. Earth Syst.*
- 1282 Davis, C. A. (2015), The formation of moist vortices and tropical cyclones in idealized
1283 simulations, *J. Atmos. Sci.*, *72*, 3499–3516, doi:10.1175/JAS-D-15-0027.1.
- 1284 Emanuel, K., A. A. Wing, and E. M. Vincent (2013), Radiative-convective instability, *J.*
1285 *Adv. Model. Earth Syst.*, *5*, doi:10.1002/2013MS000270.
- 1286 Feng, Z., S. Hagos, A. K. Rowe, C. D. Burleyson, M. N. Martini, and S. P. de Szoeke
1287 (2015), Mechanisms of convective cloud organization by cold pools over tropical warm
1288 ocean during the AMIE/DYNAMO field campaign, *J. Adv. Model. Earth Syst.*, *7*, doi:
1289 10.1002/2014MS000384.
- 1290 Frank, W. M., and P. E. Roundy (2006), The role of tropical waves in tropical cyclogenesis,
1291 *Mon. Wea. Rev.*, *134*, 2397–2417.
- 1292 Fuchs, Ž., S. L. Sessions, and D. Raymond (2014), Mechanisms controlling the on-
1293 set of simulated convectively coupled Kelvin waves, *Tellus A*, *66*, 22107, doi:
1294 10.3402/tellusa.v66.22107.
- 1295 Gjorgjievska, S., and D. J. Raymond (2014), Interaction between dynamics and ther-
1296 modynamics during tropical cyclogenesis, *Atmos. Chem. Phys.*, *14*, 3065–3082, doi:
1297 10.5194/acp-14-3065-2014.
- 1298 Held, I. M., R. S. Hemler, and V. Ramaswamy (1993), Radiative-convective equilibrium
1299 with explicit two-dimensional moist convection, *J. Atmos. Sci.*, *50*, 3909–3927.
- 1300 Herman, M. J., and D. J. Raymond (2014), Wtg cloud modeling with spectral decompo-
1301 sition of heating, *J. Adv. Model. Earth Syst.*, *06*, doi:10.1002/2014MS000359.

- 1302 Jeevanjee, N., and D. M. Romps (2013), Convective self-aggregation, cold pools, and
1303 domain size, *Geophys. Res. Lett.*, *40*, 1–5, doi:10.1002/grl.50204.
- 1304 Khairoutdinov, M., and K. Emanuel (2013), Rotating radiative-convective equilibrium
1305 simulated by a cloud-resolving model, *J. Adv. Model. Earth Syst.*, *5*, 816–825, doi:
1306 10.1002/2013MS000253.
- 1307 Khairoutdinov, M. F., and K. Emanuel (2010), Aggregated convection and the regulation
1308 of tropical climate, paper presented at the 29th Conference on Hurricanes and Tropical
1309 Meteorology, Am. Meteor. Soc., Tucson, Ariz.
- 1310 Kiladis, G. N., M. C. Wheeler, P. T. Haertel, K. H. Straub, and P. E. Roundy
1311 (2009), Convectively coupled equatorial waves, *Reviews of Geophysics*, *47*(2), doi:
1312 10.1029/2008RG000266, rG2003.
- 1313 Lindzen, R. S., and S. Nigam (1987), On the role of sea surface temperature gradients in
1314 forcing low-level winds and convergence in the tropics, *J. Atmos. Sci.*, *44*, 2418–2436.
- 1315 Majda, A. J., and B. Khouider (2001), Stochastic and mesoscopic models for tropical
1316 convection, *Proc. Natl. Acad. Sci.*, *99*, 1123–1128.
- 1317 Mapes, B. (2000), Convective inhibition, subgrid-scale triggering energy, and stratiform
1318 instability in a toy tropical wave model, *J. Atmos. Sci.*, *57*, 1515–1535.
- 1319 Mapes, B., and R. Neale (2011), Parameterizing convective organization to escape the
1320 entrainment dilemma, *J. Adv. Model. Earth Syst.*, *3*, doi:10.1029/2011MS000042.
- 1321 Masunaga, H. (2012), Short-term versus climatological relationship between precipitation
1322 and tropospheric humidity, *J. Climate*, *25*, 7983–7990, doi:10.1175/JCLI-D-12-00037.1.
- 1323 McFarlane, S. A., J. H. Mather, and T. P. Ackerman (2007), Analysis of tropical radiative
1324 heating profiles: A comparison of models and observations, *J. Geophys. Res.*, *112*,

- 1325 D14,218, doi:10.1029/2006JD008290.
- 1326 Muller, C. J., and I. M. Held (2012), Detailed investigation of the self-aggregation of con-
1327 vection in cloud-resolving simulations, *J. Atmos. Sci.*, *69*, 2551–2565, doi:10.1175/JAS-
1328 D-11-0257.1.
- 1329 Neelin, J. D., and I. M. Held (1987), Modeling tropical convergence based on the moist
1330 static energy budget, *Mon. Weat. Rev.*, *115*, 3–12.
- 1331 Nilsson, J., and K. A. Emanuel (1999), Equilibrium atmospheres of a two-
1332 column radiative-convective model, *Q. J. R. Meteorol. Soc.*, *125*, 2239–2264, doi:
1333 10.1002/qj.49712555814.
- 1334 Nolan, D. S., E. D. Rappin, and K. A. Emanuel (2007), Tropical cyclogenesis sensitivity to
1335 environmental parameters in radiative-convective equilibrium, *Q. J. R. Meteorol. Soc.*,
1336 *133*, 2085–2107, doi:10.1002/qj.170.
- 1337 Parodi, A., and K. Emanuel (2009), A theory for buoyancy and velocity scales in deep
1338 moist convection, *J. Atmos. Sci.*, *66*, 3449–3463, doi:10.1175/2009JAS3103.1.
- 1339 Peters, O., and J. D. Neelin (2006), Critical phenomena in atmospheric precipitation, *Nat.*
1340 *Phys.*, *2*, 393–396, doi:10.1038/nphys314.
- 1341 Polvani, L. M., and A. H. Sobel (2002), The Hadley circulation and the weak temperature
1342 gradient approximation, *J. Atmos. Sci.*, *59*, 1744–1752.
- 1343 Posselt, D. J., S. C. van den Heever, and G. L. Stephens (2008), Trimodal cloudiness and
1344 tropical stable layers in simulations of radiative convective equilibrium, *Geophys. Res.*
1345 *Lett.*, *35*, L08,802, doi:10.1029/2007GL033029.
- 1346 Posselt, D. J., S. C. van den Heever, G. L. Stephens, and M. R. Igel (2012), Changes in
1347 the interaction between tropical convection, radiation, and the large-scale circulation in

- 1348 a warming environment, *J. Climate*, *25*, 557-571, doi:10.1175/2011JCLI4167.1.
- 1349 Raymond, D., . Fuchs, S. Gjorgjievska, and S. Sessions (2015), Balanced dynamics and
1350 convection in the tropical troposphere, *Journal of Advances in Modeling Earth Systems*,
1351 doi:10.1002/2015MS000467.
- 1352 Raymond, D. J. (2001), A new model of the Madden-Julian Oscillation, *J. Atmos. Sci.*,
1353 *58*, 2807–2819.
- 1354 Raymond, D. J., and Z. Fuchs (2007), Convectively coupled gravity and moisture
1355 modes in a simple atmospheric model, *Tellus*, *59A*, 627–640, doi:10.1111/j.1600-
1356 0870.2007.00268.x.
- 1357 Raymond, D. J., and S. L. Sessions (2007), Evolution of convection during tropical cyclo-
1358 genesis, *Geophys. Res. Lett.*, *34*, L06,811, doi:10.1029/2006GL028607.
- 1359 Raymond, D. J., and X. Zeng (2000), Instability and large scale circulations in a two-
1360 column model of the tropical troposphere, *Quart. J. Roy. Meteor. Soc.*, *126*, 3117–3135.
- 1361 Raymond, D. J., and X. Zeng (2005), Modelling tropical atmospheric convection in the
1362 context of the weak temperature gradient approximation, *Quart. J. Roy. Meteor. Soc.*,
1363 *131*, 1301–1320.
- 1364 Raymond, D. J., G. B. Raga, C. S. Bretherton, J. Molinari, C. López-Carrillo, and Z. Fuchs
1365 (2003), Convective forcing in the intertropical convergence zone of the eastern Pacific,
1366 *J. Atmos. Sci.*, *60*, 2064–2082.
- 1367 Raymond, D. J., S. L. Sessions, and Z. Fuchs (2007), A theory for the spinup of tropical
1368 depressions, *Q. J. Roy. Meteor. Soc.*, *133*, 1743–1754.
- 1369 Raymond, D. J., S. L. Sessions, A. H. Sobel, and . Fuchs (2009), The mechanics
1370 of gross moist stability, *Journal of Advances in Modeling Earth Systems*, *1*(3), doi:

- 1371 10.3894/JAMES.2009.1.9, 9.
- 1372 Raymond, D. J., S. L. Sessions, and C. L. Carrillo (2011), Thermodynamics of trop-
1373 ical cyclogenesis in the northwest Pacific, *J. Geophys. Res.*, *116*, D18,101, doi:
1374 10.1029/2011JD015624.
- 1375 Robe, F. R., and K. A. Emanuel (2001), The effect of vertical wind shear on radiative-
1376 convective equilibrium states, *J. Atmos. Sci.*, *58*, 1427–1445.
- 1377 Romps, D. M. (2012a), Weak pressure gradient approximation and its analytic solutions,
1378 *J. Atmos. Sci.*, *69*, 2835–2845, doi:10.1175/JAS-D-11-0336.1.
- 1379 Romps, D. M. (2012b), Numerical tests of the weak pressure gradient approximation, *J.*
1380 *Atmos. Sci.*, *69*, 2846–2856, doi:10.1175/JAS-D-11-0337.1.
- 1381 Sentic, S., S. L. Sessions, and Z. Fuchs (2015), Diagnosing convection with weak temper-
1382 ature gradient simulations of DYNAMO, *J. Adv. Model. Earth Syst.*, Accepted Author
1383 Manuscript, doi:10.1002/2015MS000531.
- 1384 Sessions, S. L., S. Sugaya, D. J. Raymond, and A. H. Sobel (2010), Multiple equilibria in a
1385 cloud resolving model using the weak temperature gradient approximation, *J. Geophys.*
1386 *Res.*, *115*, D12110, doi:10.1029/2009JD013376.
- 1387 Sessions, S. L., M. J. Herman, and S. Sentić (2015), Convective response to changes in
1388 the thermodynamic environment in idealized weak temperature gradient simulations,
1389 *J. Adv. Model. Earth Syst.*, *7*, 712–738, doi:10.1002/2015MS000446.
- 1390 Sobel, A. H., and C. S. Bretherton (2000), Modeling tropical precipitation in a single
1391 column, *J. Climate*, *13*, 4378–4392.
- 1392 Sobel, A. H., G. Bellon, and J. Bacmeister (2007), Multiple equilibria in a single-
1393 column model of the tropical atmosphere, *Geophys. Res. Lett.*, *34*, L22,804, doi:

- 1394 10.1029/2007GL031320.
- 1395 Stephens, G. L., S. van den Heever, and L. Pakula (2008), Radiative-convective feedbacks
1396 in idealized states of radiative-convective equilibrium, *J. Atmos. Sci.*, *65*, 3899–3916,
1397 doi:10.1175/2008JAS2524.1.
- 1398 Su, H., C. S. Bretherton, and S. S. Chen (2000), Self-aggregation and large-scale control
1399 of tropical deep convection: A model study, *J. Atmos. Sci.*, *57*, 1797–1816.
- 1400 Tobin, I., S. Bony, and R. Roca (2012), Observational evidence for relationships between
1401 the degree of aggregation of deep convection, water vapor, surface fluxes, and radiation,
1402 *J. Climate*, *25*, 6885–6903, doi:10.1175/JCLI-D-11-00258.1.
- 1403 Tompkins, A. M. (2001a), On the relationship between tropical convection and sea surface
1404 temperature, *J. Climate*, *14*, 633–637.
- 1405 Tompkins, A. M. (2001b), Organization of tropical convection in low vertical wind shears:
1406 The role of water vapor, *J. Atmos. Sci.*, *58*, 529–545.
- 1407 Tompkins, A. M., and G. C. Craig (1998), Radiative-convective equilibrium in a three-
1408 dimensional cloud-ensemble model, *Q. J. R. Meteorol. Soc.*, *124*, 2073–2097.
- 1409 Wang, S., and A. H. Sobel (2011), Response of convection to relative sea surface temper-
1410 ature: cloud-resolving simulations in two and three dimensions, *J. Geophys. Res.*, *116*,
1411 D11,119, doi:10.1029/2010JD015347.
- 1412 Wang, S., and A. H. Sobel (2012), Impact of imposed drying on deep convection in a
1413 cloud-resolving model, *J. Geophys. Res.*, *117*, D02112, doi:10.1029/2011JD016847.
- 1414 Wang, S., A. H. Sobel, and Z. Kuang (2013), Cloud-resolving simulation of TOGA-
1415 COARE using parameterized large scale dynamics, *J. Geophys. Res.*, *118*, 6290–6301,
1416 doi:10.1002/jgrd.50510.

1417 Wing, A. A., and T. W. Cronin (2015), Self-aggregation of convection in long channel
1418 geometry, *Q. J. R. Meteorol. Soc.*, doi:10.1002/qj.2628.

1419 Wing, A. A., and K. A. Emanuel (2013), Physical mechanisms controlling self-aggregation
1420 of convection in idealized numerical modeling simulations, *J. Adv. Mod. Earth Sys.*, 5,
1421 1–14, doi:10.1002/2013MS000269.

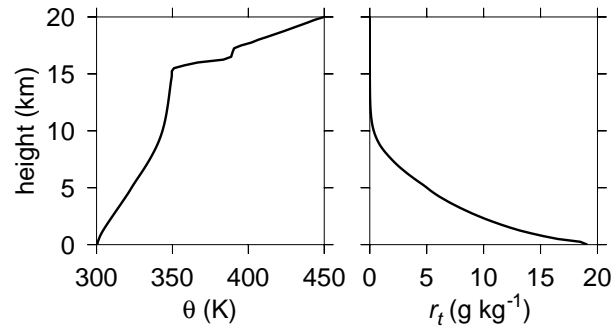


Figure 1. Radiative convective equilibrium (RCE) profiles of potential temperature (left) and total water mixing ratio (right) used as unperturbed reference profiles in WTG calculations. RCE is calculated over a uniform SST of 303 K, with surface wind speed of 5 ms^{-1} and interactive radiation on a 2D, 200 km horizontal domain. See text for more details. Reprinted with permission from *Sessions et al.* [2015].

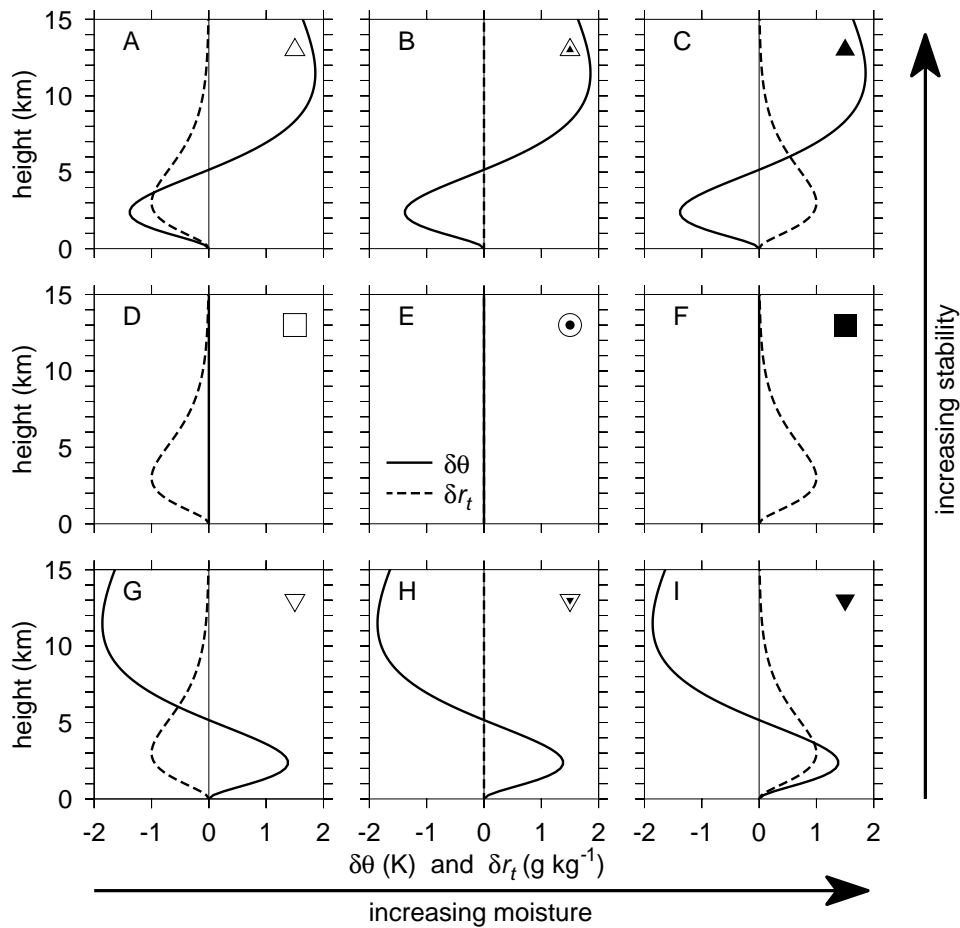


Figure 2. Perturbations added to the RCE reference profile. Solid lines represent perturbations to the potential temperature profiles, dotted lines give mixing ratio perturbations. The symbols in the upper right of each panel is a geometric representation of the thermodynamic environment where the shape corresponds to atmospheric stability and the shading corresponds to atmospheric moisture. Columns going from left to right have increasing moisture in the reference environment; in analogy with a glass of water, drier environments have empty symbols, unperturbed r_t profiles are half-filled, moister profiles are filled. Atmospheric stability increases from the bottom row to the top, and is represented by the geometric stability of the shape: more unstable environments have inverted triangles, unperturbed θ profiles have neutrally stable squares, more stable environments have upright triangles. In order to easily distinguish when neither θ or r_t is perturbed (center panel), we use bulls-eyes. This figure serves as a legend for the results presented

Figure 2. (continued)

in section 4. It is reprinted with permission from *Sessions et al.* [2015].

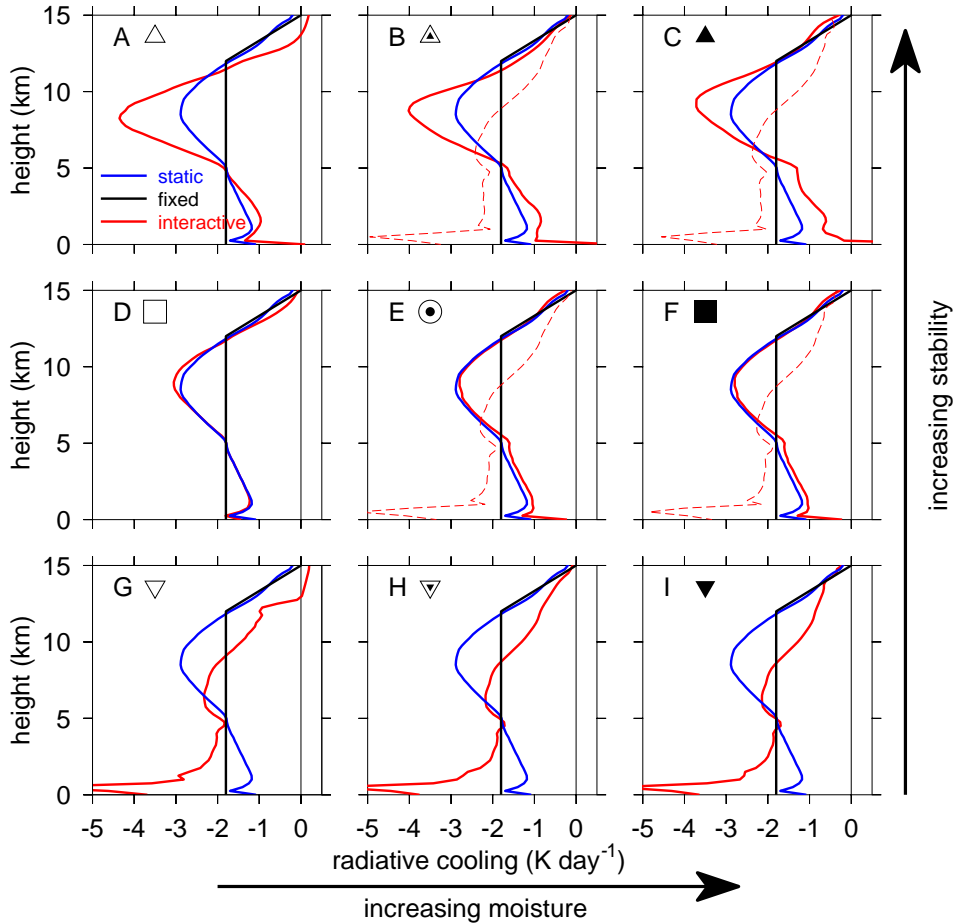


Figure 3. Radiative cooling profiles for each thermodynamic environment. Black and blue lines represent fixed (-1.8 K day^{-1}) and static (mean cooling profile from RCE simulation) cooling profiles. These are the same for all experiments. Red lines show the cooling profiles when radiation cools interactively. The thin dashed lines in (bcef) are cooling profiles in multiple equilibria runs where an initially dry troposphere remains dry. The symbols in the upper left corners are the geometric representation of the thermodynamic environments shown in figure 2.

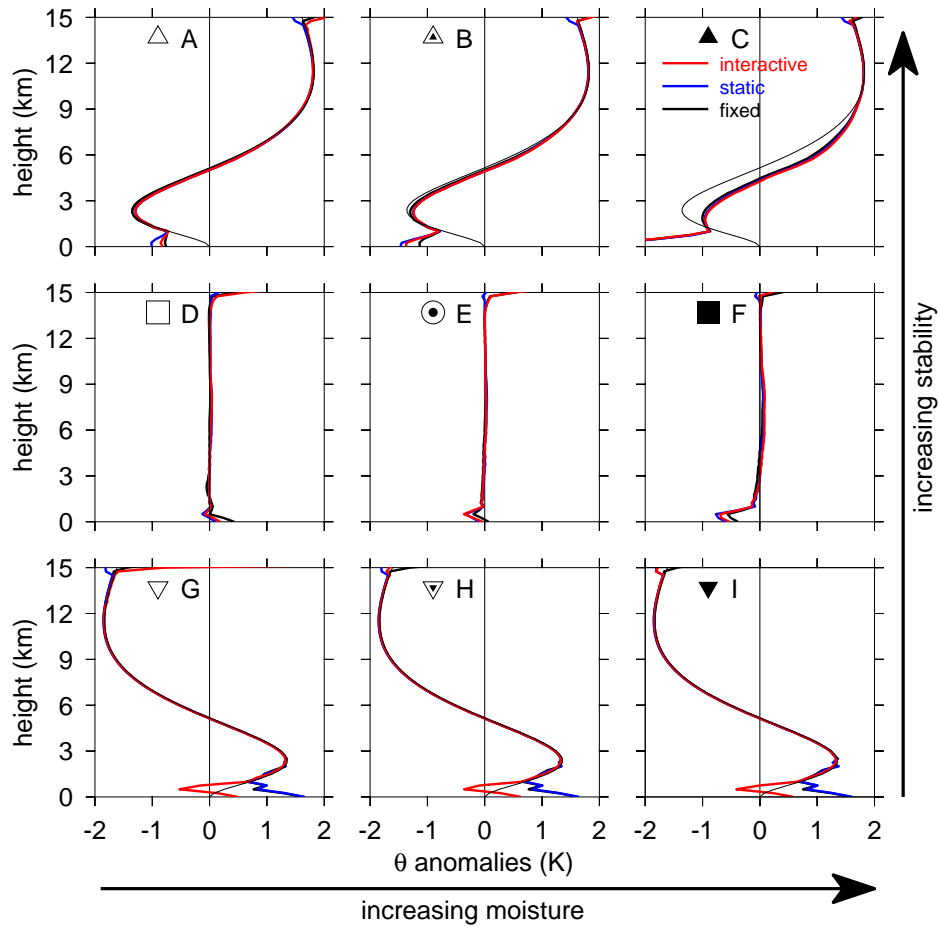


Figure 4. Potential temperature anomalies. The colors represent the different radiation treatments. The thin black line shows the potential temperature anomaly applied to the reference profile (same as the θ anomalies in figure 2).

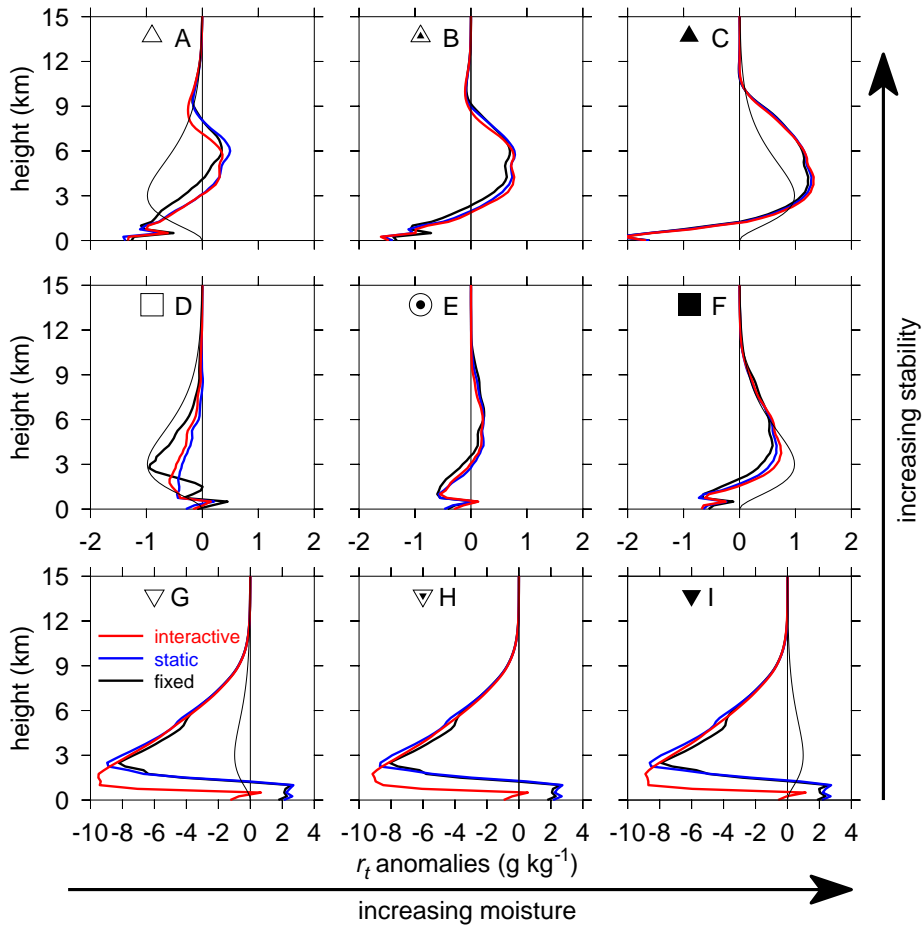


Figure 5. Total water mixing ratio anomalies. As in figure 4, the color represent the different radiation treatments. Note the different horizontal scale on the bottom row (g-i) compared to the top two rows (a-f). All horizontal tic marks represent increments of 2 g kg⁻¹.

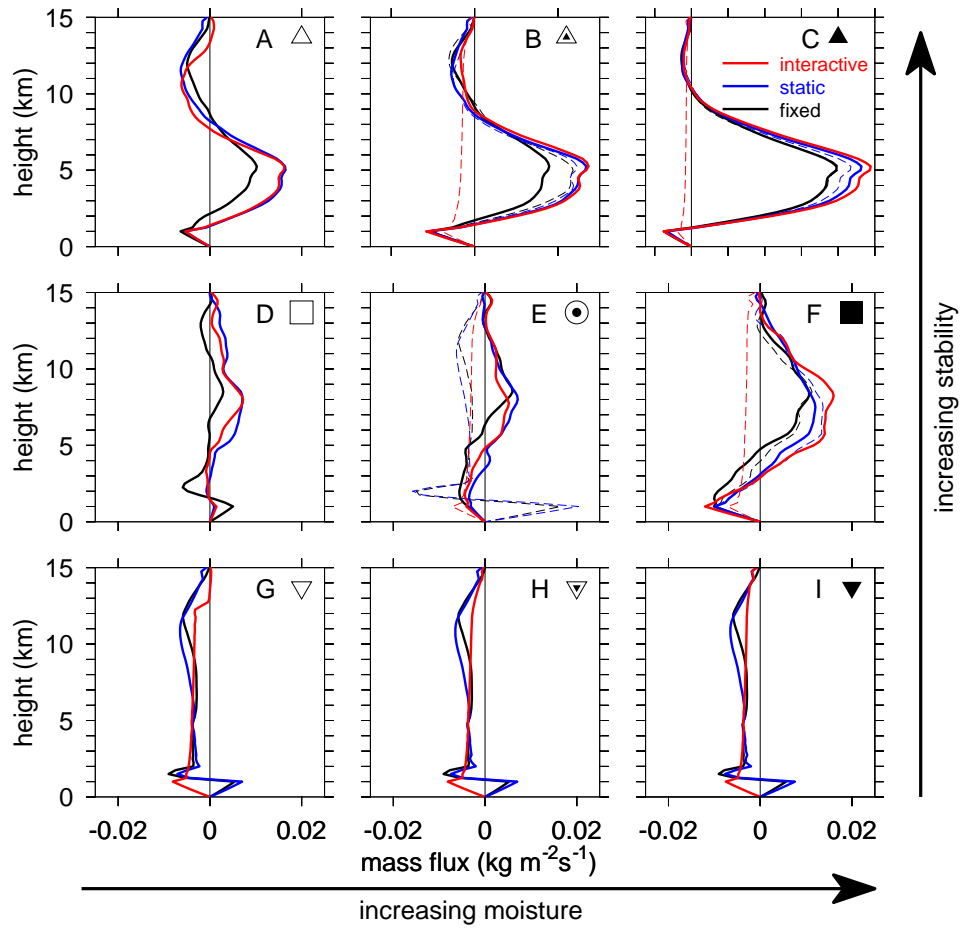


Figure 6. Mass flux profiles for different radiation treatments (distinguished by color) in different thermodynamic environments. Dashed lines show results when simulations are initiated with dry tropospheres (for multiple equilibria experiments, section 2.4). Note the different horizontal scales in the top row (a-c) compared to the bottom two rows (d-i). Tic marks represent $0.02 \text{ kg m}^{-2}\text{s}^{-1}$ increments.

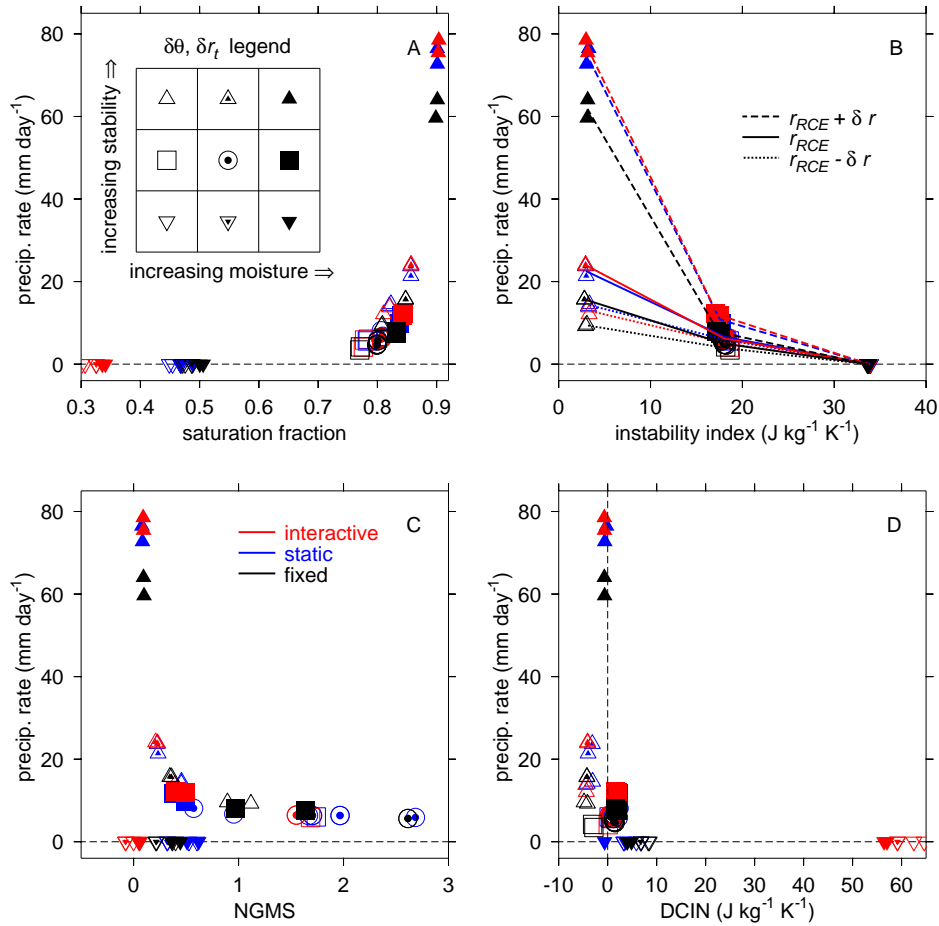


Figure 7. Precipitation rate as a function of (a) saturation fraction, (b) instability index, (c) NGMS, and (d) DCIN. Each symbol represents time and domain averages for simulations corresponding to different reference temperature and moisture profiles. The legend embedded in (a) corresponds to the perturbations shown in figure 2. The colors correspond to radiation treatment. The lines in (b) connect experiments with identical reference moisture profiles.

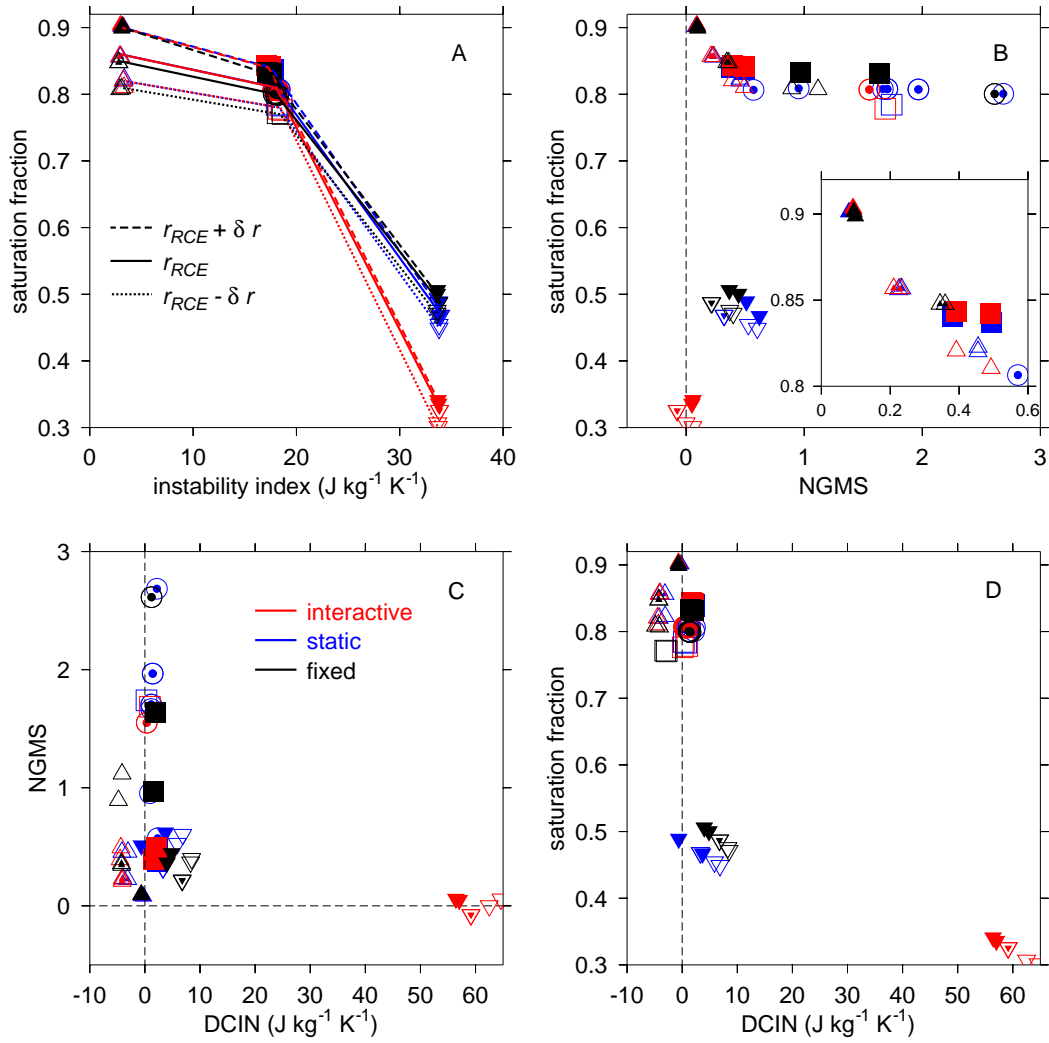


Figure 8. Relationships between convective diagnostics. (a) Saturation fraction versus instability index, (b) saturation fraction versus NGMS, (c) NGMS versus DCIN, and (d) saturation fraction versus DCIN. The symbol legend is the same as that in figure 7, colors represent radiation treatment. Lines in (a) connect experiments with identical reference moisture profiles. The inset in (b) is an amplification of (b) showing high saturation fractions and low NGMS.

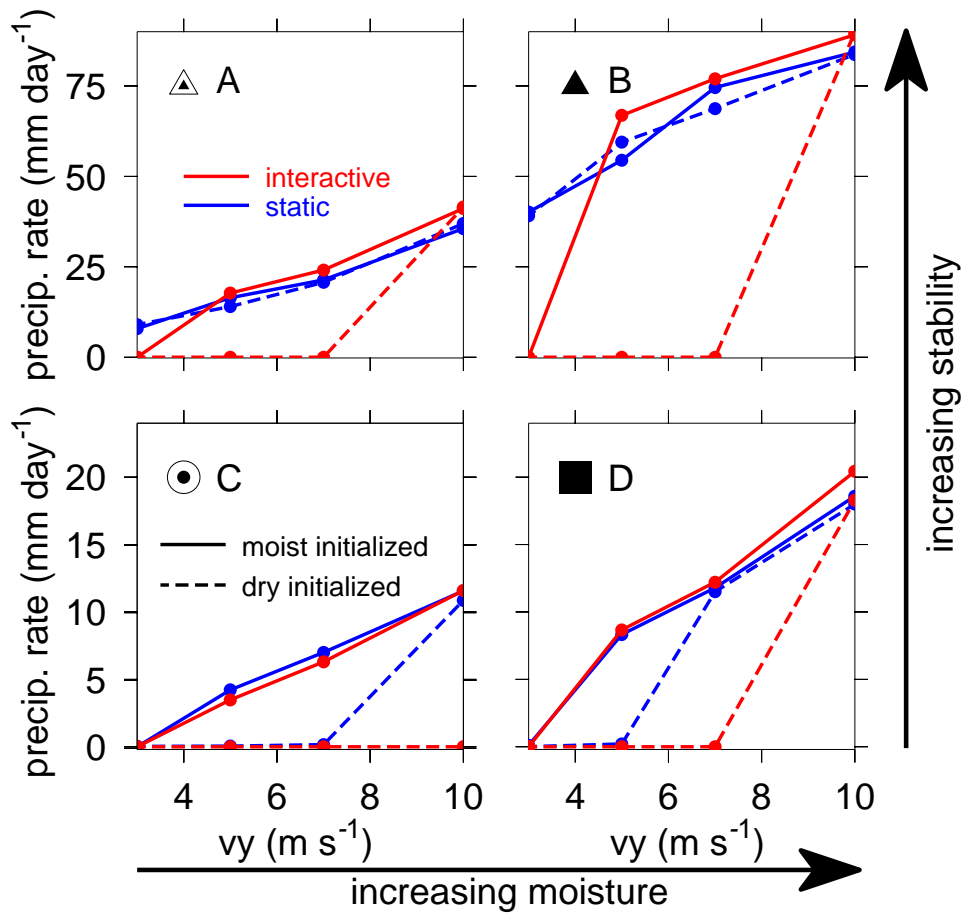


Figure 9. Precipitation rate as a function of surface wind speed, v_y , for different reference environments: (a) more stable, (b) more stable and moister, (c) unperturbed, and (d) moister. Solid lines correspond to simulations initialized with the reference moisture profile, dashed lines represent initially dry simulations. Blue lines are results for static radiation; red represents simulations with interactive radiation. Multiple equilibria exist when dashed lines show zero precipitation rate while solid lines have non-zero rates.

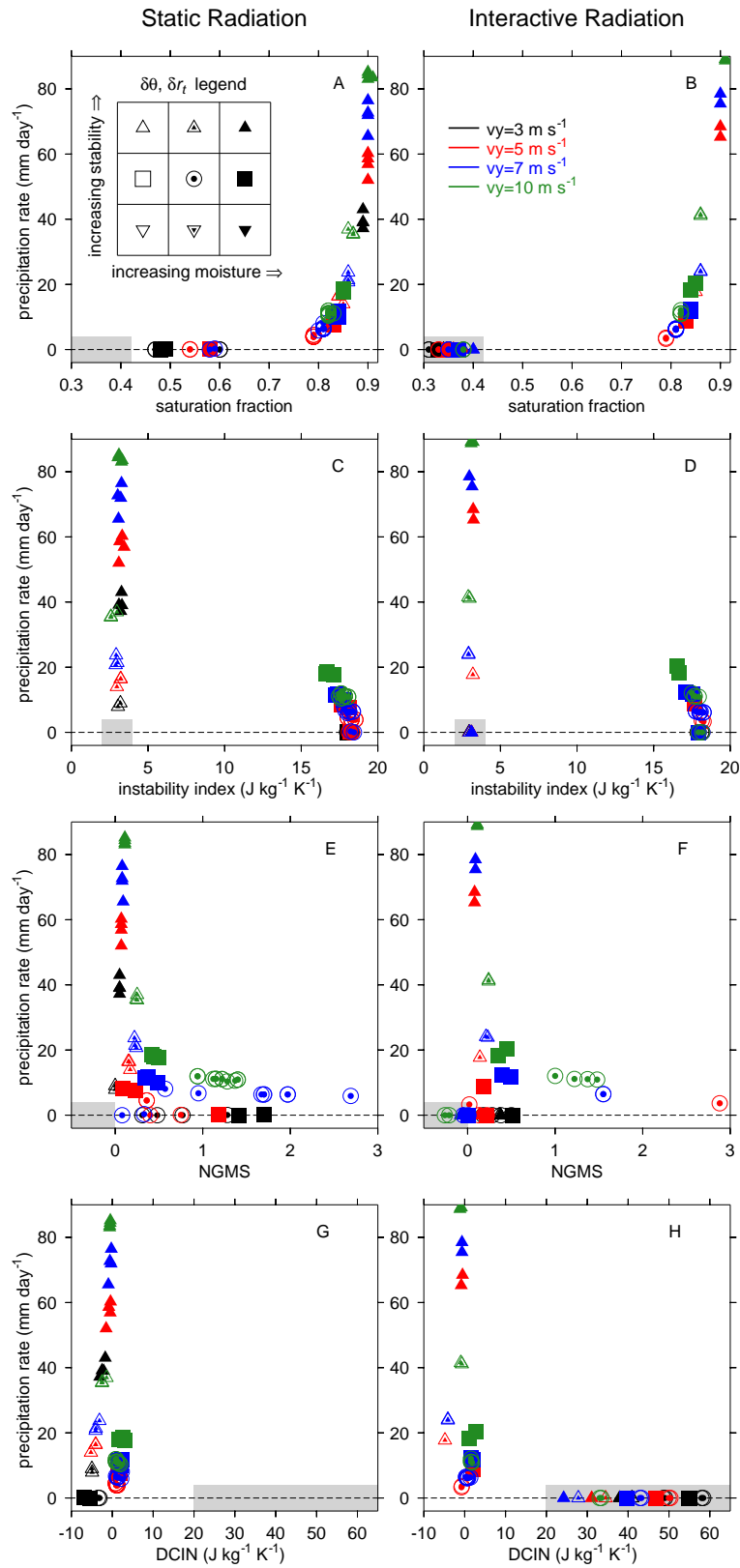


Figure 10. Scatterplots exhibiting the relationships between precipitation and (a,b) saturation fraction, (c,d) instability index, (e,f) NGMS, and (g,h) DCIN. Symbols

Figure 10. (continued)

correspond to the reference environments defined in figure 2, with a symbol legend as an inset in (a). Colors represent surface wind speeds used in each experiment. The left column (a,c,e,g) are results using static radiation; the right column (b,d,f,h) are results with interactive radiation. Significant differences between static and interactive radiation are highlighted with gray shading.